INO/2004/01

Brief Project Report

INDIA-BASED NEUTRINO OBSERVATORY

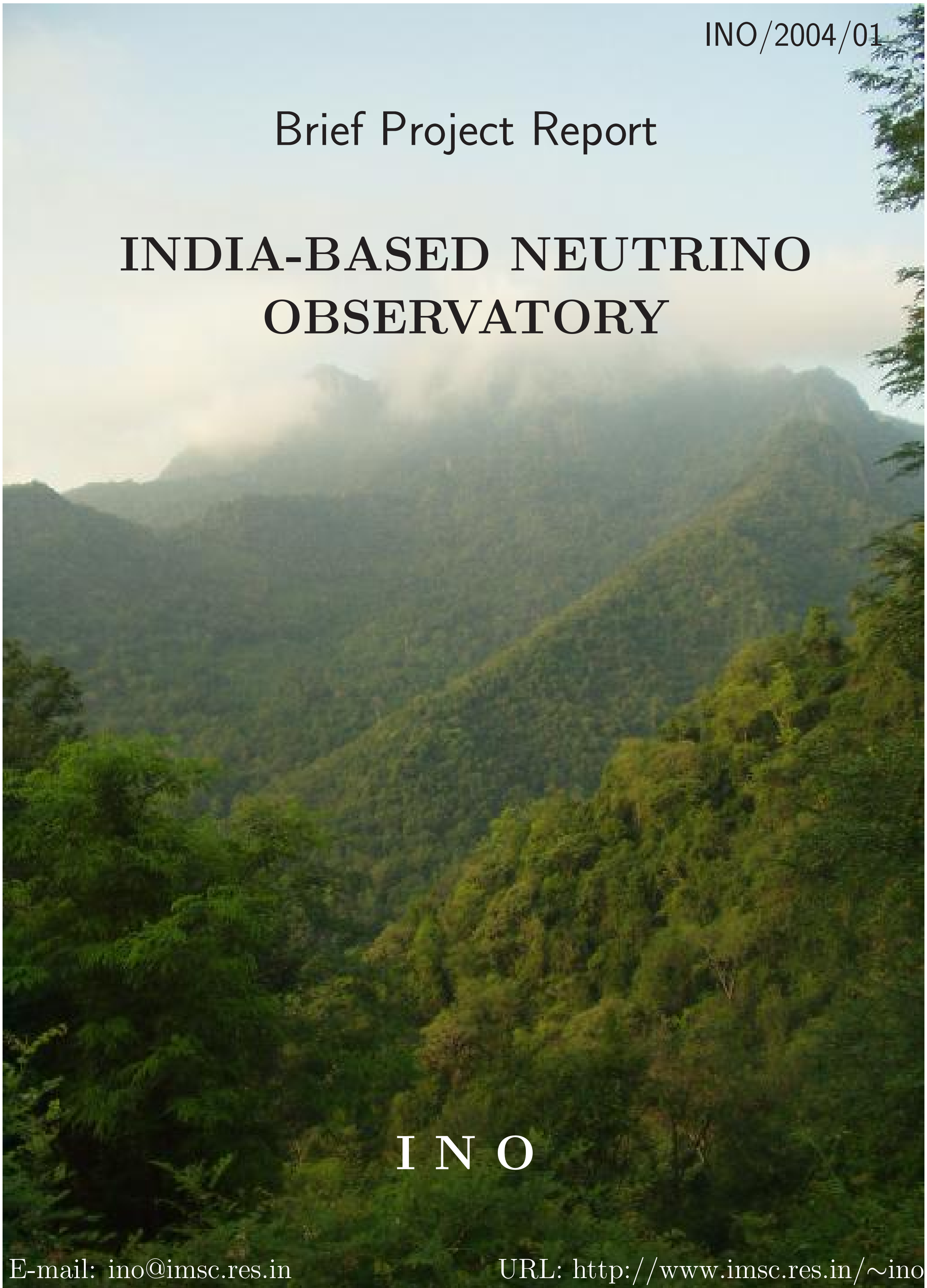

I N O

E-mail: ino@imsc.res.in URL: http://www.imsc.res.in/∼ino

PREFACE

Very important developments have occurred recently in neutrino physics and neutrino astronomy. Oscillations of neutrinos and the inferred discovery that neutrinos have mass are likely to have far-reaching consequences. This discovery has come from the study of solar and cosmic ray produced neutrinos.

The pioneering solar neutrino experiments of Davis and collaborators in USA, the gigantic Super-Kamiokande detector in Japan, the heavy-water detector at the Sudbury Neutrino Observatory in Canada, and a few other laboratories, together, have contributed in a very fundamental way to our knowledge of neutrino properties and interactions. In particular, the Canadian experiment has given direct experimental proof of the 80-year-old hypothesis that the Sun and the stars are powered by thermonuclear fusion reactions.

Impelled by these discoveries and their implications for the future of particle physics, plans have been made—world-wide—for new neutrino detectors, neutrino factories and long base-line neutrino experiments.

India was a pioneer in neutrino experiments. In fact cosmic ray produced neutrinos were first detected in the deep mines of Kolar Gold Fields (KGF) in 1965.

It is planned to revive underground neutrino experiments in India. A multi-institutional National Neutrino Collaboration has been formed with the objective of creating an India-based Neutrino Observatory (INO).

The feasibility study for this project is in progress and an Interim Report based on the study is nearing completion. What follows is a short report that summarises the main issues and questions that the collaboration would like to address. More details may be found on the INO web-site: http://www.imsc.res.in/∼ino.

Contents

1 Introduction and overview **1**

1.1 Current Status of neutrino physics experiments 2

1.2 Overview of the INO report 5

2 The ICAL Detector **9**

2.1 ICAL: A magnetised iron calorimeter with fast timing 9

2.1.1 Detector Structure 10

2.1.2 Active Detector Elements: RPCs 10

2.1.3 Present Status of RPC R & D 11

2.1.4 Magnet Design 13

2.2 Design capacity of magnetised ICAL detector 14

3 Physics Issues **15**

3.1 Three flavour neutrino oscillation 16

3.2 Parameter values gleaned from experiments so far 17

3.3 Atmospheric Neutrinos 18

3.3.1 Observing the oscillation pattern 19

3.3.2 Matter effects in atmospheric μ^-/μ^+ events 20

3.3.3 Discrimination between $\nu_\mu \to \nu_\tau$ and $\nu_\mu \to \nu_s$ 23

3.3.4 Probing CPT Violation 25

3.3.5 Constraining long-range leptonic forces 26

3.4 Neutrino Factories 27

3.4.1 Determination of θ_{13} 27

3.4.2 Sign of δ_{32} 28

3.4.3 Probing CP violation in leptonic sector 31

3.4.4 Detecting Large Matter Effects in $\nu_\mu \to \nu_\tau$ Oscillations 33

3.5 Other physics possibilities 33

4 Numerical Simulations on ICAL **37**

4.1 Events generation 37

4.2 The detector simulations package 38

4.3 Event reconstruction 38

4.3.1 Muon energy reconstruction 39

4.3.2 Muon direction reconstruction 39

4.3.3 Muon charge identification 40

4.3.4 Hadron energy calibration 42

4.4 Study of atmospheric neutrino events 43

4.4.1 Analysis with horizontal detector plates 43

4.4.2 Analysis with vertical detector plates 45

5 Tale of two (three) sites 51
5.1 Site Requirements 51
5.2 Summary of the sites 52
5.3 Tunnel and Cavern Complex 56
5.4 Comparison of PUSHEP and Rammam 57

6 Strategies for Human Resource Development 61

7 Cost and Time Schedules 63
7.1 Cost Factors 63
7.2 Time Scale 65

8 INO as a facility for the future 67

Chapter 1

Introduction and overview

Neutrino physics has come to occupy the centre stage of high energy physics, after the discovery of non-vanishing neutrino mass by observations of atmospheric neutrinos at the Super-Kamiokande underground laboratory in Japan as well as from observations of solar neutrinos at Super-Kamiokande [3] and the Sudbury Neutrino Observatory in Canada [2].

Neutrino physics is one of the fastest evolving fields in physics today. Neutrinos, introduced by Pauli in 1930, were first predicted to explain the continuous electron energy distribution in nuclear beta decay. Their name is due to Enrico Fermi who, in 1934, made them the basis for a theory of weak interactions. It was clear very early that these particles would be difficult to observe because of their very small cross sections. But in a series of experiments Reines and Cowan conclusively proved their existence through the inverse beta decay weak interaction process where an *electron-type* antineutrino $\overline{\nu}_e$ is captured by a proton p giving rise to a positron e^+ and a neutron n: $\bar{\nu}_e + p \rightarrow e^+ + n$.

Apart from electron-type neutrinos which are produced in nuclear beta decay, the separate identity of *muon-type* neutrinos ν_μ was proved in 1962. The discovery of the τ lepton a decade later implied the existence of a third *tau-type* neutrino, ν_τ. It was only in the year 2001 that its existence was directly observed. A result of fundamental importance to neutrino physics is the precise measurement of the decay width of the Z-boson which is saturated by (and hence indicates the existence of only) three active light neutrino flavours.

The sources of naturally occurring neutrinos are both terrestrial and extraterrestrial. They are also produced in the laboratory. Each of these sources provides information, sometimes overlapping, that is extremely important in understanding the intrinsic properties of the neutrinos and their sources. The energy spectrum of naturally produced neutrinos starts from fractions of electron-volts and spans an impressive range. Fig. 1.1 shows the spectra of neutrinos from different sources as a function of their energies. Some of the spectra shown are based on observation while others, especially at high energies, are based on model calculations. While no single detector can fathom such a large range in energy, the very fact that neutrinos are produced over such a wide energy range poses challenging problems in their detection and understanding.

In the "Standard Model" (SM) of particle physics, neutrinos are massless and come in three distinct *types* or *flavours*, ν_e, ν_μ, ν_τ. These interact only via weak interactions and hence are difficult to detect. In the SM there is no room for neutrino flavours to "oscillate" into each other. If, however, neutrinos have mass, and, furthermore, the neutrino *flavour* eigenstates which participate in the weak interactions are mixtures of *mass* eigenstates with different masses, then quantum mechanical evolution of these flavour states leads to the phenomenon

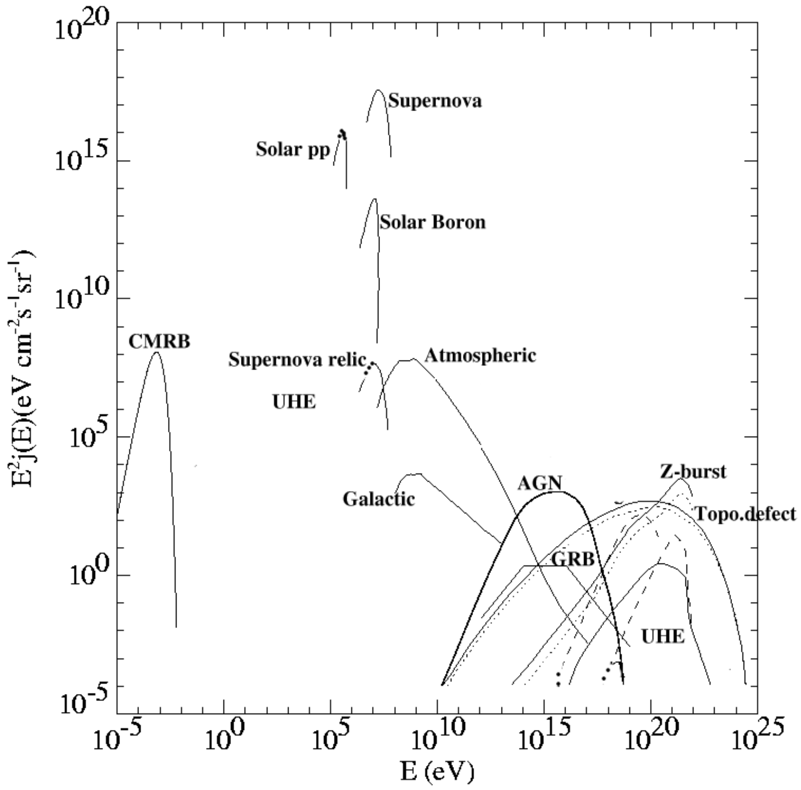

Figure 1.1: Neutrino spectra from different sources as a function of energy [4].

of neutrino oscillations [1]. Experiments on solar neutrinos [2] and atmospheric neutrinos [3] clearly indicate that neutrinos do exhibit such flavour oscillations. Such experiments constrain the extent of mixing as well as the squared differences of the three masses. In particular, while the absolute masses themselves are not constrained by such experiments, at least two of the neutrinos must be massive, and with different masses, for consistency of the theory with observed data. This is in fact the first evidence for physics beyond the Standard Model of particle physics. However, the estimated smallness of the neutrino mass (of the order of eV or much smaller) may have its origins near or beyond the scale of grand unified theories (GUTs), thus probing physics beyond the reach of present day accelerators.

1.1 Current Status of neutrino physics experiments

Experiments in the last several decades have provided many new and significant results. The main results may be summarised as follows:

- **Solar and Atmospheric neutrinos**: The observation of the deficit in electron neutrinos from the Sun constitutes the Solar Neutrino problem. The combination of deficit in charged current interactions (involving only electron neutrinos) and the lack thereof in neutral current interactions (involving all neutrino flavours identically) indicates that the solution to this problem is through neutrino oscillations. The best solution implies a mass squared difference of $\delta_{\text{solar}} \sim 8 \times 10^{-5}$ eV^2 and fairly large mixing. The other problem involves the atmospheric muon neutrinos, whose deficit is accounted for by a mass squared difference $\delta_{\mathrm{atm}} \sim 2 \times 10^{-3}$ eV^2 [6, 7], more than an order of magnitude larger than the mass-squared difference relevant to solar neutrino data, and yet another large mixing between states. These observations thus imply the existence of at least two non-zero masses for neutrino mass eigenstates.

- **Beta decay and double beta decay**: In contrast to neutrino oscillation-sensitive experiments, these yield direct mass limits. So far, there is only an upper limit of 2.2 eV on the dominant mass eigenstate for electron neutrinos involved in tritium beta decay. Several planned experiments such as KATRIN will be capable of improving the limit to 0.3 eV. The limits from experiments involving muon and tau-type neutrinos are much higher and may not be relevant in the light of present information on neutrino oscillations.

  Neutrino-less double decay experiments address the issue of whether the neutrino is a Majorana or Dirac particle (whether or not it is its own antiparticle). If neutrinos are indeed Majorana particles, data from the experiments limit their mass to less than 0.2 eV. Future neutrino-less double beta decay experiments such as GENIUS are capable of pushing the Majorana neutrino mass limit to 0.01 eV [5].

- **Cosmological data**: Cosmological experiments, including data from the recent WMAP experiment, apart from limiting the number of light neutrino flavour, set an upper limit on the sum of all the active neutrino masses, $\sum_i m_{\nu_i} < 0.7$ eV.

- **Neutrinos from Supernova**: The observation of neutrinos from the Supernova SN1987a [8] has confirmed many qualitative features of the stellar collapse scenario. However, the number of observed events are statistically too small to draw conclusions on the properties of the neutrinos.

- **Other neutrino properties**: Stringent upper limits also exist for neutrino magnetic moments, life times, and other such properties. Future experiments like MUNU will futher improve the limit on the neutrino magnetic moment [9].

A summary of the present status of masses and mixings is shown in Fig. 1.2 as obtained from a combined analysis of the pioneering experiments conducted at Homestake, Sudbury, Kamioka, CHOOZ and KamLAND laboratories. Note that we have chosen $m_3^2 - m_1^2 > 0$ in this figure; the so-called direct mass hierarchy. The present data does not distinguish between the two possible hierarchies: $m_3^2 > m_2^2 > m_1^2$ (direct), $m_2^2 > m_1^2 > m_3^2$ (inverted). Also, this figure does not include the unusual results obtained by the LSND Collaboration in Los Alamos laboratory [10], which are yet to be confirmed by an independent experiment.

In spite of these remarkable results, there are several outstanding issues of fundamental importance:

1. While there is definite evidence for the non-vanishing mass of neutrinos, the oscillation pattern itself, that is visible periodic changes in the neutrino flux with oscillation minima and maxima, has not been seen explicitly. A recent Super-Kamiokande [11] analysis clearly shows a dip, indicating that the first oscillation minimum has been observed at the 3σ level; hence the oscillation hypothesis remains a strong contender to explain the various anomalies.

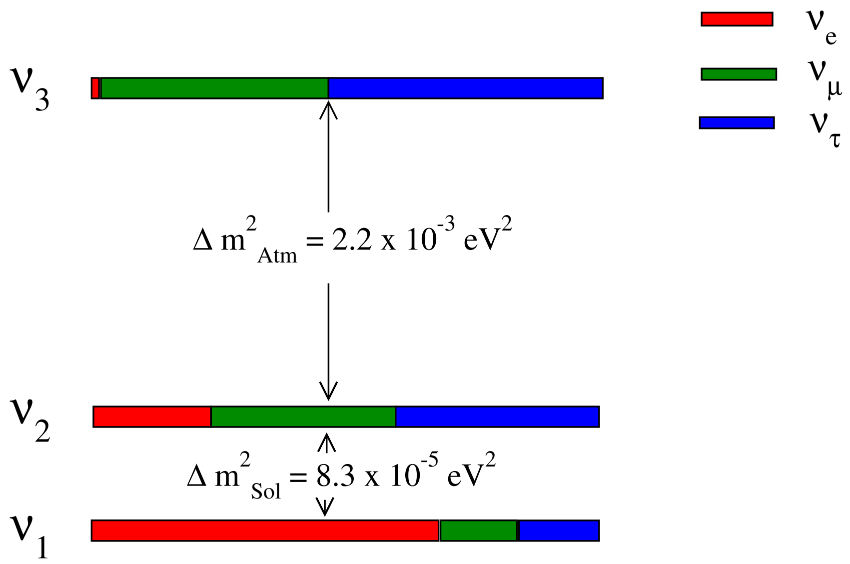

Figure 1.2: Schematic illustration of the status of masses and mixings of neutrino mass eigenstates. The flavour content is indicated by different colours. The direct mass hierarchy is assumed here; in the case of the inverted hierarchy, the ν_3 state would be the lightest.

2. Analysis of solar and atmospheric neutrino data indicate that there are two large mixing angles. These imply that (1) the ν_μ and ν_τ states have large contributions from all three mass eigenstates while (2) the ν_e state is virtually saturated by the ν_1 and ν_2 mass eigenstates with large individual contributions; that is, the admixture of ν_3 in ν_e as parametrised by the 1–3 mixing angle, θ_{13}, is small, with $\sin^2 2\theta_{13} < 0.13$ (3σ). However (modulo the LSND data), it is not known whether this angle is different from zero.

3. The mass hierarchy of neutrinos is not known. Assuming a three flavour scenario, matter effects clearly indicate both the magnitude and sign of the mass squared difference occurring in the solar neutrino problem. Since ν_es are involved here, this translates to knowing the magnitude and sign of $\delta_{21} = m_2^2 - m_1^2$ due to the arguments given above. It turns out that δ_{21} is positive.

   The atmospheric neutrino data and indeed any reactor or base-line experiment is so far insensitive to the sign of the mass squared difference between the participating neutrinos. Hence the sign of $\delta_{31} = m_3^2 - m_1^2$ is not yet known; this is the hierarchy problem. This can be determined through matter effects as the neutrinos propagate through the earth.

4. Is there CP violation in the leptonic sector? It is known that these effects are small; however, this is a question of fundamental and deep significance which may be probed in future long-baseline neutrino experiments.

5. Do neutrinos decay? While this is unlikely as a dominant scenario to explain the known anomalies, it may still be allowed in combination with neutrino oscillations, the latter being the dominant mechanism.

6. What is the absolute scale of neutrino mass? Direct mass measurements from electron beta decay place an upper limit of about 2.2 eV. Interpretation of the recent astrophysical results from WMAP [12] limits the sum of the neutrino masses to around 0.7 eV. Neutrino-less double beta decay, if observed, will also determine the mass scale.

7. Are the neutrinos Dirac or Majorana particles? There is a strong theoretical prejudice that neutrinos are Majorana particles, that is, they are their own antiparticles. Only charge-neutral fermions (spin-1/2 particles) can be Majorana and hence neutrinos are the only candidates within the Standard Model. Hence there is great interest in establishing this by an unambiguous observation of neutrino-less double beta decay.

8. How many species of neutrinos exist? The number of active species with masses less than half the mass of the Z boson is limited to three by LEP experiments. Results from the LSND experiment suggests the existence of at least one more relatively light species, which has to be sterile (that is, cannot experience weak interactions), since there cannot be more than three light active species. Results from MiniBOONE are awaited to confirm or rule out the LSND results.

9. Does the neutrino have a non-zero magnetic moment? The existence of a magnetic moment for neutrinos is of fundamental importance (for example, a non-zero magnetic moment is possible only if the neutrino mass is nonzero). It will also have an impact on the solar neutrino problem. Several experiments have already placed upper limits on the magnetic moment of antineutrinos in the region 2–4 $\times 10^{-10}\mu_B$ and this limit needs to be improved further.

Both at Sudbury and Kamioka the low energy solar neutrino experiments are still going on as also at Gran Sasso. Low energy reactor neutrino experiments are going on at laboratories such as KamLAND and CHOOZ. The low energy experiments are expected to give a nearly complete understanding of neutrino properties at this scale in not too distant a future. The atmospheric neutrino studies are expected to be augmented by those on GeV neutrinos produced and beamed from accelerators (or neutrino factories) at FNAL, KEK and CERN. Some of the experiments being planned are at existing sites such as Gran Sasso, Kamioka, etc. In order to take measurements at several distances from neutrino factories, many long base-line stations are also being planned. Some of the on-going and future detectors along with some of their important characteristics are mentioned in Table 1.1.

One of these detectors, called MONOLITH [13], designed as a 30 kton iron calorimeter, has the capability of unambiguously establishing atmospheric neutrino oscillations as well as studying neutrinos from CERN. The current proposal for an iron calorimeter detector, ICAL, at INO is based substantially on this idea.

1.2 Overview of the INO report

Historically the Indian initiative in cosmic ray and neutrino physics goes back several decades. As a result of extensive studies of the muon flux at several depths in the Kolar Gold mines,

Experiment	Country	Type of detector	Major goals	Time schedule
Super-Kamiokande	Japan	Water Cerenkov	Solar, Supernova, Atmospheric, Long-baseline(K2K)	1996-
SNO	Canada	D_2O Cerenkov	Solar, Supernova	1999–
GNO	Italy	Gallium	Solar	1998–
ICARUS	Italy	Liquid Argon	Atmospheric, Proton Decay, Long-baseline	?
KamLAND	Japan	Scintillator	Reactor	2001–
Double-CHOOZ	France	Scintillator	Reactor	2007
MiniBooNE	USA	Scintillator	Short baseline, Fermilab booster	2003–
MINOS	USA	Iron Calorimeter	Long baseline, Fermilab injector	2005
OPERA	Italy	Lead/Emulsion	Tau appearance	2005
MONOLITH	?	Iron Calorimeter	Atmospheric, Long-baseline	?

Table 1.1: On-going and planned large scale neutrino experiments [14].

it was realised that the muon flux was low enough to permit measurements on atmospheric neutrinos. The first ever such neutrino interaction which was observed as early as in 1965 was at Kolar [15]. This laboratory later looked for nucleon decay and placed upper limits on the half-life of the proton [16]. Another interesting observation was that of the so-called Kolar events, which have not been explained to date [17]. These suggested a decaying heavy particle with an amazingly long lifetime of a few nanosececonds.

Most of these experiments were done using iron calorimeters weighing up to 300 tons, with visual detectors (such as neon flash tubes) and proportional counters. Unfortunately the mines were closed down in 1990 and these experiments were discontinued. Such experiments helped, however, in acquiring an expertise with iron calorimeter detectors. In view of the importance of neutrino physics as outlined above and the past Indian contribution, it has long been felt that the Indian efforts in neutrino physics should be revived.

Considering the physics possibilities and given the past experience at Kolar, it was decided, after a prolonged discussion, to start with a modern iron calorimeter (ICAL) with Resistive Plate Chambers (RPCs) as the active detector elements. The detector, to be described in the next chapter, is to be housed in low-background surroundings at a suitable place. There is world-wide interest in this type of detector and a quick implementation of such a project can achieve many physics goals such as:

- Unambiguous and more precise determination of **oscillation parameters** using atmospheric neutrinos.

- Study of **matter effects** through charge identification, that may lead to the determination of the unknown sign of one of the mass differences.

- High-precision determination of the oscillation parameters when ICAL is (perhaps upgraded and) used in the future as a far-end detector for a **long base-line neutrino oscillation** experiment.

- Study of **charge-conjugation and parity (CP) violation** in the leptonic sector as well as possible **charge-conjugation, parity, time-reversal (CPT) violation** studies.

- Study of **Kolar events**, possible identification of **ultra-high energy** neutrinos and **multi-muon** events.

Details of the physics possibilities are presented in Chapter 3. Results of numerical simulations of some of the physics issues at ICAL and the energy, time and direction resolution of such a detector are presented in Chapter 4.

The geographical location for any India-based neutrino laboratory is particularly interesting, as most of the neutrino detectors are scattered around the world at latitudes above 35°. There is none close to the equator as yet. It is possible to push such a detector down to almost 8° latitude in South India. Such a location permits neutrino astronomy searches covering the whole celestial sky, study of solar neutrinos passing through the Earth's core and finally neutrino tomography of the Earth at a future date using terrestrial and laboratory neutrino sources. Hence, although INO will start its activity with the ICAL detector, it is envisaged that it will ultimately have other neutrino experiments as well under its umbrella. Indeed, electron neutrino detection (as an addition to ICAL or as a separate detector) opens up several possibilities for future directions including the augmentation of any long baseline program, or solar, supernova and geoneutrino studies.

A summary of the geology and related issues of two possible sites for locating INO, namely Singara in the Nilgiris and Rammam in the Darjeeling Himalayas are discussed in Chapter 5.

A project of the magnitude that is envisaged needs to draw on considerable human resources. Strategies for tapping the resources already available but distributed weakly over India, as well as training more manpower, is a vital issue. Futhermore, international collaboration, especially for the future long base-line efforts, is a desirable feature. Some discussions and possible options are discussed in Chapter 6.

Given the world-wide interest and the number of experiments planned and proposed in this field, and in order to obtain results from ICAL that are competitive with those from other experiments, it is critical to construct the ICAL detector in a time-bound and phased manner. Cost and times estimates, both for constructing the INO lab as well as constructing and housing the ICAL detector are given in Chapter 7. A strict adherence to these time-lines is necessary both to have relevance in the field and to keep costs in check.

This brief report concludes in Chapter 7 with a discussion of the general issues pertaining to an underground laboratory. We give a list of relevant reviews and websites at the end from which more information on the neutrino experiments and theory may be obtained.

INO [19] has been conceived on a scale that no other basic sciences project in India has attempted. The MoU signed by seven Institutions, that brought the National Neutrino Collaboration (NNC) group into existence, is already the first of its kind. It is a result of the enthusiasm shown by the neutrino physics community in India. The interest shown by the international community in this project is also encouraging. Over time INO is expected to develop into a full-fledged underground science laboratory hosting experiments that require low background environment, including other disciplines such as geology and biology, that can profit from its special environment and infrastructure.

Chapter 2

The ICAL Detector

NOTE: TOO BRIEF, ESP MAGNET DESIGN

With the goal of atmospheric and long baseline neutrino physics in view, two basic detector types were discussed by the INO group. They are the **water Cerenkov detector**, such as the existing Super-Kamiokande detector in Japan, and a **magnetised iron calorimeter**, which would be an extension of and improvement over the old KGF detector [16] and similar in design to the proposed MONOLITH [13] detector.

In order to resolve some of the issues thrown up by Super-K, it will be necessary to go in for a very large water detector, of the order of one megaton. This type of detector design is well-known and quite straightforward. However, the active detector elements, photo-multiplier tubes, need to be developed in this country.

The magnetised iron calorimeter (ICAL) design has RPCs as the active detector element. This major component of the detector is still in the R&D stage. The most interesting feature of this detector is that the magnetic field, in addition to improving range and resolution of energy, will be able to separate differently charged particles; for example, it will distinguish μ^+ from μ^-. This is crucial not only for CP violation studies but also to study earth matter effects on atmospheric neutrinos as well as being an absolute necessity for the far-end detector of a long base-line experiment such as is feasible at INO with the neutrino beam from a neutrino factory, in Japan or elsewhere.

2.1 ICAL: A magnetised iron calorimeter with fast timing

ICAL is mostly sensitive to muons produced in the interaction of muon neutrinos (and anti-neutrinos) with the detector material. We therefore focus on issues related to muon detection. Of particular relevance are the energy and direction measurements of the muons. The calorimeter can also measure the energy of hadron(s) produced in the charged-current interaction of interest. These measurements will, in effect, be a measure of the energy and direction of the initial neutrino. These measurements are directly relevant to a study of neutrino oscillation parameters. Thus can be understood from a simplified (two-flavour) model of neutrino oscillations where the survival probability of atmospheric muon neutrinos is (see the next chapter for more details),

$$P_{\mu\mu} = 1 - \sin^2 2\theta \sin^2 \left(\frac{1.27 \delta L}{E} \right) , \tag{2.1}$$

where L is the distance travelled in km and E is the energy of the neutrino in GeV. Here θ, the neutrino mixing angle and δ, the difference of the neutrino mass squared eigenvalues expressed in eV^2, are the oscillation parameters of interest. Clearly the survival probability is an oscillating function of L/E within this approximation. A verification of the oscillation hypothesis thus requires an identification of the minima and maxima. The most recent analysis of Super-K events shows evidence for the first dip in $P_{\mu\mu}$. Although this measurement is very suggestive of muon neutrino oscillation, only an observation of the full oscillation pattern as a function of L/E over at least one period will constitute a confirmation of the oscillation scenario. This requires a detector which extends over a large range of L/E with good E and L resolution (which requires an accurate measurement of the position and direction). These goals can be achieved by a good tracking calorimeter.

In such a detector the energy of the neutrinos can be measured very accurately by detecting fully and partially contained events with the vertex inside the detector. Energy of fully contained events can be measured by track length methods whereas for partially contained events, the energy of the escaping muon can be well estimated from the bending of its track in the magnetic field within the detector. The path length L, of the neutrino can be estimated from the muon direction. Furthermore, the oscillation pattern is clearly defined by a certain ratio, in a fixed L/E bin, of events from up-coming and down-going neutrinos, as will be discussed in the next chapter. A sub-nano-second time resolution, which ensures an almost perfect up-down discrimination of the event, is necessary for this. Thus a detector with a large mass with good timing characteristics and with a magnetic field satisfies the requirement for such measurements.

2.1.1 Detector Structure

The proposed detector, see Fig. 2.1, will have two modules of lateral sizes 16 m $\times$ 16 m each and a height of about 12 m. This is composed of 140 layers of iron plates of thickness 6 cm each,[1] inter-leaved with active detector elements placed in air-gaps of thickness 2.5 cm each, as described in the next subsection. The iron plates can be magnetised to 1–1.4 Tesla. The total mass of such a detector including the support structure, etc., will be approximately 35 kton. The plates can, in principle, be arranged horizontally or vertically depending on whether one is more interested in near vertical or horizontal neutrinos. The whole detector as described above is to be surrounded by an external layer of scintillation counters. This will act as a veto layer and will be used to identify muons entering the detector from outside as well as to identify partially confined events with vertex inside the detector. In addition to the main detector, the possibility of locating, at a later stage, two smaller detectors of equal area but with fewer layers of active detector elements on either side of the main detector to increase the aperture to neutrinos from astrophysical objects, is being studied.

2.1.2 Active Detector Elements: RPCs

The total active area of the detector is 32×16 m^2 between two successive planes, or a total of 70,000 square meters for the whole detector. Glass Spark Chambers (GSC) or Resistive Plate Chambers (RPC) which are low-cost active detectors [20] with nano-second timing resolution are well suited to span such a large area. The RPC, shown in Fig. 2.2, is a gas filled detector

[1] While this has been assumed throughout, note that it 6.3 cm is the manufacturing standard. In the event of using 6.3 cm plates, the simulation results are expected to change only marginally.

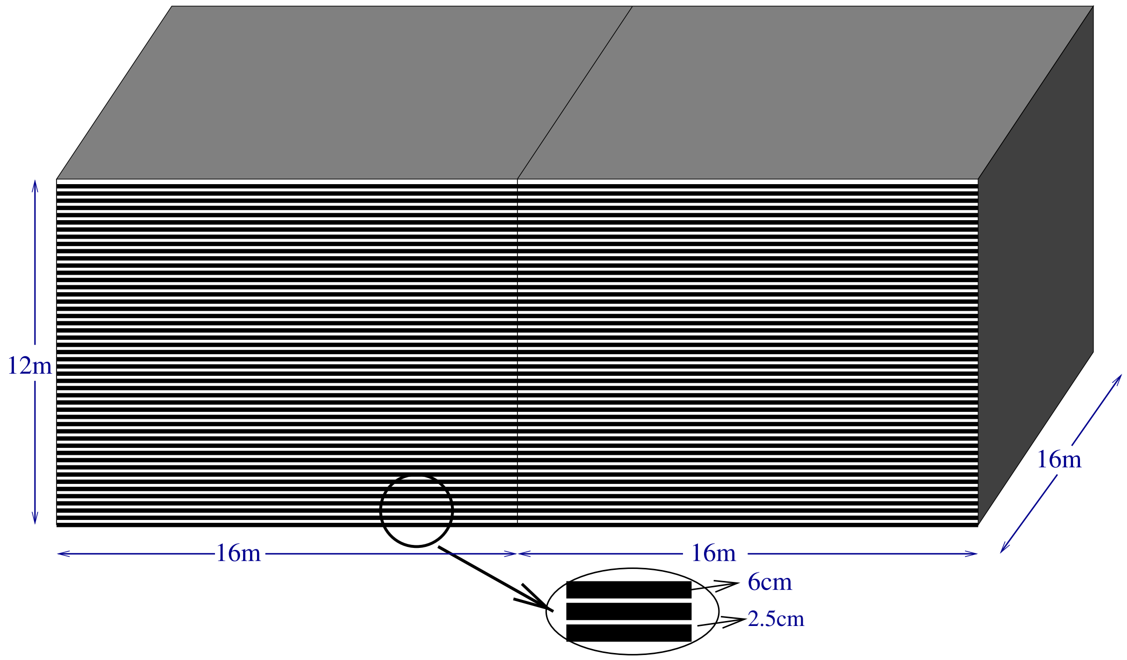

Figure 2.1: Sketch of the iron calorimeter detector.

with two parallel electrodes of 2 mm thick float glass, having a volume resistivity of 10^{12} ohm-cm, kept 2 mm apart by suitable spacers. For a suitable electrical field and combination of gas mixture (of argon, freon and isobutane) contained within the chamber, the detector operates in a spark mode. The high resistivity of the electrodes and the choice of the gas mixture ensure the containment of the spark as well as the short recovery time. The high voltage (in the range of 8–10 kV) is applied to the electrodes either by means of graphite coating or resistive adhesive film on the glass plate.

A basic RPC detector element is 2 m in length and 2 m wide. Eight such RPC elements cover a road of 16 m $\times$ 2 m and are read out by 64 pickup strips along the x direction (2 m wide road) and 512 strips along the y direction (16 m). There are a total of 16 roads in a layer, see Fig. 2.3. The strip pickup planes can be realised by glueing a grooved copper foil on one side of a plastic honey-comb, the other side of which has a continuous foil and is grounded. It can also be realised by using a copper clad G10 sheet with readout strips grooved on one side with the other side acting as the ground plane. A spatial accuracy of about 1.5 cm on both views can be obtained with such a read out.

The thickness of the detector tray to be inserted between two iron plates is about 2 cm. The total number of GSC units required is about 18,000. Thus detector fabrication is a gigantic task due to the scale and requires active participation from industry.

2.1.3 Present Status of RPC R & D

Prototype RPCs have been built at TIFR and SINP. An advanced gas mixing unit has been designed at SINP with many built-in features for gas mixing. A major milestone has been reached with the efficiency crossing 90% above 8.6 kV applied voltage. In Fig. 2.4 the performance of the prototype at TIFR is shown. Apart from the efficiency, the other important

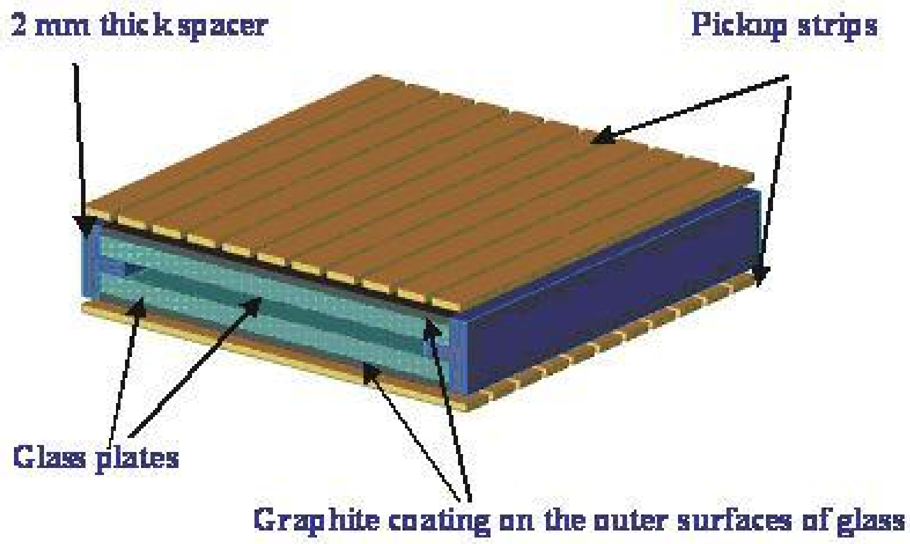

Figure 2.2: Sketch of a typical glass spark chamber.

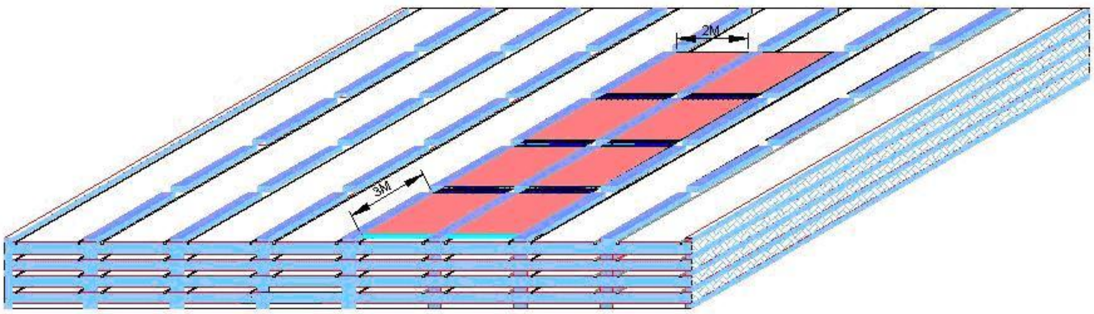

Figure 2.3: Basic detector elements: strip planes.

feature of this detector element is the fast timing which is necessary for discriminating the up-going muons from the down-going ones. Furthermore, as shown in Fig. 2.5, the timing is as good as or better than in the case of a scintillator detector.

The detector R & D is currently focussing on the following issues:

- RPC timing, charge distribution, noise and cross-talk.
- Mean charge vs voltage relationship, which appears to be linear.
- Gas composition and mixing. At present three gases are being used in the mixture

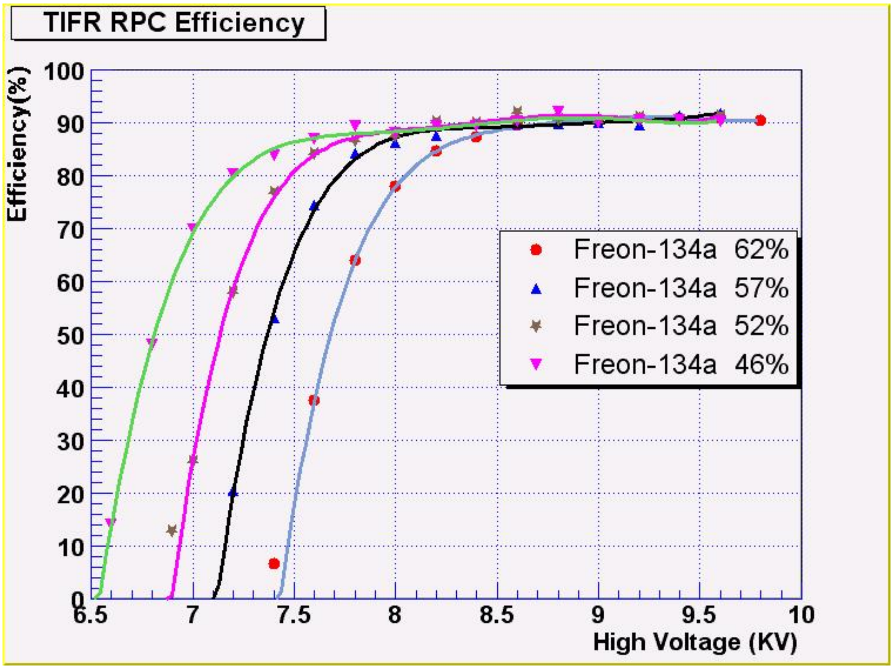

Figure 2.4: RPC efficiency as a function of HV for different gas compositions.

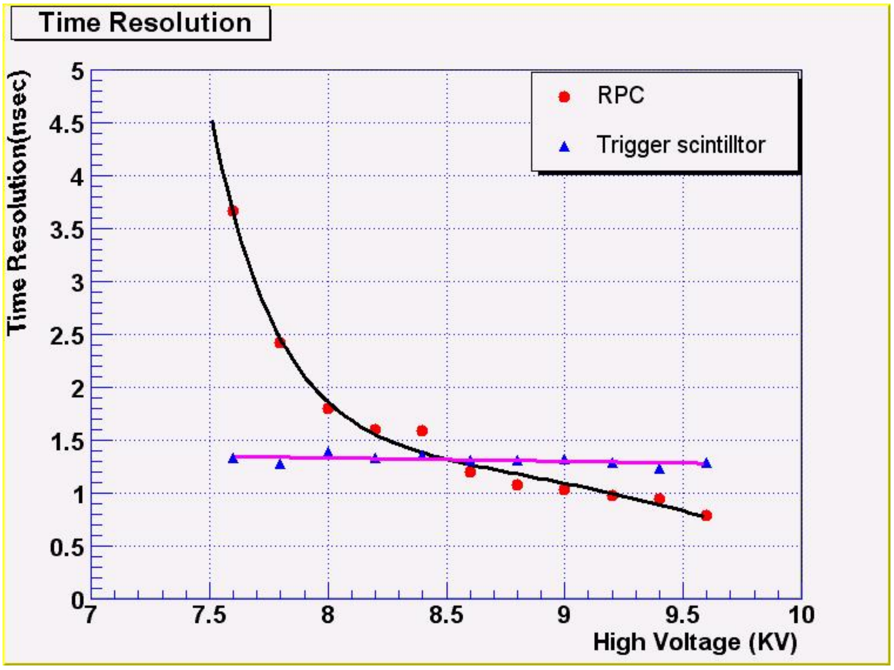

Figure 2.5: Comparison of the time resolution of the RPC and Scintillator.

with the concentration of isobutane kept at 8%. The content of freon 134 and argon are varied as shown in Fig. 2.4.

2.1.4 Magnet Design

The design for magnetisation of ICAL is still at a very preliminary stage. The necessary software has been installed and the field mapping is in progress at BARC and VECC.

CAN WE SAY MORE ABOUT THIS ?????????????

To summarise, the main characteristic of the ICAL detector is a clean identification of muons with good energy and time (hence direction) resolution. Also, the presence of the magnetic field will distinguish positively and negatively charged particles.

2.2 Design capacity of magnetised ICAL detector

The design capacity of the ICAL has been worked out in detail and a separate report is available. The proposed detector consists of Magnetised Iron Calorimeter and Glass Spark Chamber Detector Elements. The ICAL consists of one hundred forty 60 mm steel plates stacked vertically, with 32 m × 16 m plates in plane and spaced with a 25 mm gap in between.

The bending stress and deformation of steel plates and glass plates has been checked and found to be adequate when steel spacers spaced at 2 m centre-to-centre are included for support, as shown in Fig. 2.6. The resulting configuration is shown in Fig. 2.7. The bearing width of the steel spacer and the concrete foundation has also been checked. The total load on the rock cavern due to the arrangement has been checked for the bearing capacity and is found to be adequate.

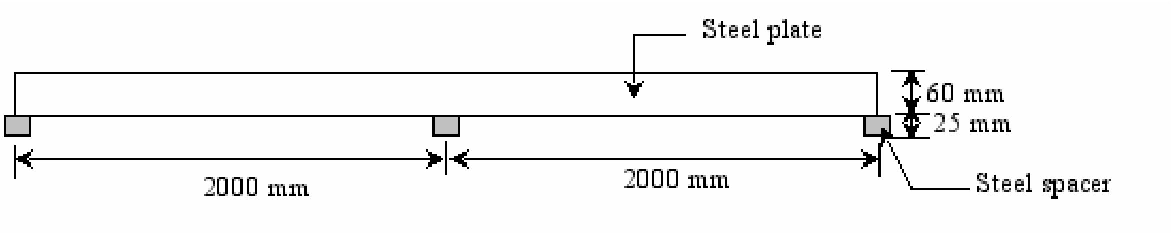

Figure 2.6: Schematic of steel structural supports for ICAL.

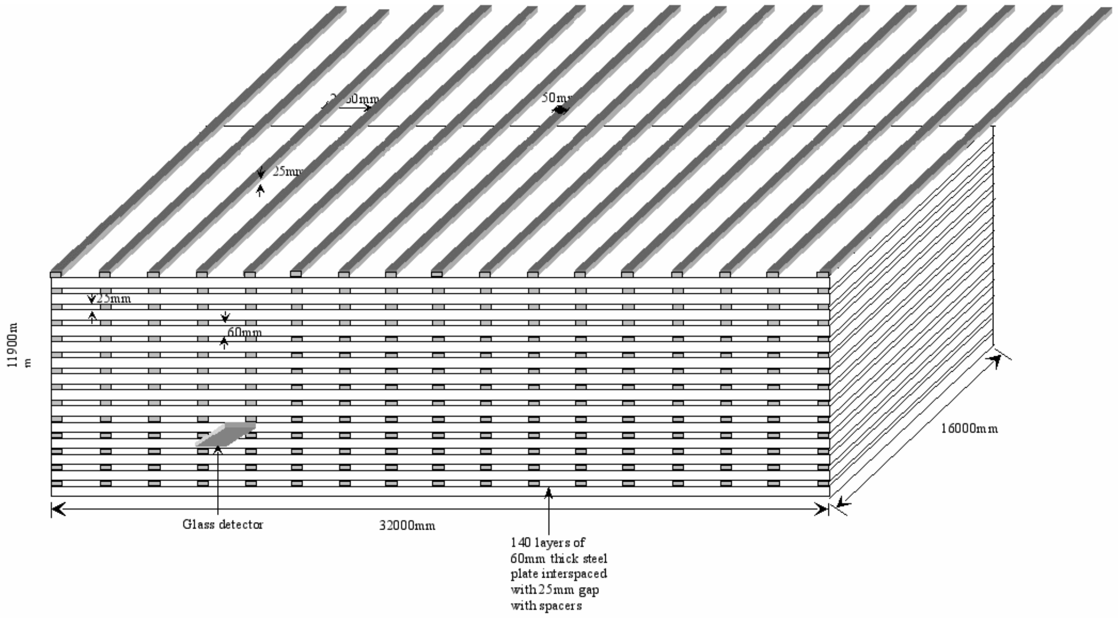

Figure 2.7: Schematic of INO including structural supports.

Chapter 3

Physics Issues

There has been a paradigm shift in the nature of the goals to be pursued in neutrino physics. From a search for an understanding of the particle physics and/or the astrophysics that drives the solar and atmospheric neutrino deficits, the focus has shifted to one where *increasingly precise measurements of neutrino mass and mixing matrix parameters* are sought. Experiments planned over the next fifteen to twenty years reflect this change in focus.

Almost all the planned projects in neutrino oscillation measurements are of the following types:

1. *a conventional proton beam* colliding with a target to produce pions and kaons which then decay to electron and muon neutrinos (and antineutrinos),

2. *super-beams*, which are essentially technologically upgraded high-flux versions of conventional beams,

3. *reactor sources* with both near and far detectors to reduce systematic errors,

4. *muon storage rings*, which exploit muon decay to produce intense and collimated neutrino beams. These are still in the R & D stage.

Experiments involving direct mass searches such as beta decay and neutrinoless double beta decay are not discussed here.

The experiments listed above will provide compelling evidence for non-zero neutrino mass and oscillations, along with ranges of possible mass and mixing parameters; more importantly, they have identified the experimental goals and directions the neutrino community must pursue over the next two decades. At this juncture the main goals of oscillation physics research are to determine the unknown oscillation parameters (mass-squared differences and mixing angles) and to improve the precision of the mass differences and mixing angles that we already know. Specifically, the aims are

- To substantiate/verify the observed oscillation dip by the Super-K collaboration and conclusively show that oscillations are responsible for observed flux deficits by observing at least one full oscillation period.

- To determine the sign of the mass-squared difference δ_{32} involved in atmospheric neutrino oscillations.

- To improve the existing upper limit on the mixing angle θ_{13} and to ascertain if its value is different from zero or not.
- To determine whether the leptonic CP phase δ is non-zero, and if so, obtain some measure of its magnitude, provided $\theta_{13} \neq 0$.
- To determine whether sterile neutrinos exist.
- Last but not the least, to probe any non-standard mechanism beyond neutrino oscillation due to non-zero mass and mixing occurring at a sub-leading level.

Different experimental facilities are being planned to improve the current bounds on the solar and atmospheric parameters as well as to improve the sensitivity to θ_{13}, the CP violating phase δ and the sign of δ_{32}. Over the next two decades, the present and next generation experiments are likely to give us useful information on the goals mentioned above.

To summarise, planned experiments will, over the next 15–20 years, greatly improve the precision on δ_{31}, effect a very modest improvement in the existing measurements for $\sin^2\theta_{23}$, and improve the upper bound on $\sin^2\theta_{13}$ by a factor of two to six, depending on the experiment. We note that these experiments, given their insensitivity to matter effects, will not be able to determine the sign of δ_{31} and thus establish whether neutrino masses follow a normal hierarchy or an inverted one. They will thus leave one of the major questions of neutrino physics unaddressed.

Some of the above challenges can be addressed in a set-up such as ICAL at INO, including the major open problem—**the sign of** δ_{31}—even with atmospheric neutrinos as source. Below we briefly describe the prospects of the ICAL detector, first for atmospheric neutrinos and subsequently using it as an end detector of a high energy high intensity neutrino beam from a distant source. In order to understand the notation and concepts used in the text we give a brief introduction to three-flavour-oscillation physics.

3.1 Three flavour neutrino oscillation

The neutrino flavour states $|\nu_\alpha\rangle$, $\alpha = e, \mu, \tau$, are linear superpositions of the neutrino mass eigenstates $|\nu_i\rangle$, $i = 1, 2, 3$, with masses m_i :

$$|\nu_\alpha\rangle = \sum_i U_{\alpha i}|\nu_i\rangle.$$

Here U is the 3×3 unitary matrix which may be parametrised (ignoring Majorana phases) [21] as:

$$U = \begin{pmatrix} c_{12}c_{13} & s_{12}c_{13} & s_{13}e^{-i\delta} \\ -c_{23}s_{12} - s_{23}s_{13}c_{12}e^{i\delta} & c_{23}c_{12} - s_{23}s_{13}s_{12}e^{i\delta} & s_{23}c_{13} \\ s_{23}s_{12} - c_{23}s_{13}c_{12}e^{i\delta} & -s_{23}c_{12} - c_{23}s_{13}s_{12}e^{i\delta} & c_{23}c_{13} \end{pmatrix}.$$

where $c_{ij} = \cos\theta_{ij}$, $s_{ij} = \sin\theta_{ij}$, and δ denotes the CP violating (Dirac) phase. By definition, the 3×3 neutrino mass matrix M_ν is diagonalised by U:

$$U^\dagger M_\nu U = \mathrm{diag}(m_1, m_2, m_3). \tag{3.1}$$

The probability of an initial neutrino ν_α of flavour α and energy E being detected as a neutrino ν_β of the same energy but with flavour β after travelling a distance L in vacuum is

$$P_{\alpha\beta} = \delta_{\alpha\beta} - 4 \sum_{i>j} \mathrm{Re}[U_{\alpha i}U^*_{\beta i}U^*_{\alpha j}U_{\beta j}] \sin^2\left(\frac{\pi L}{\lambda_{ij}}\right) + 2 \sum_{i>j} \mathrm{Im}[U_{\alpha i}U^*_{\beta i}U^*_{\alpha j}U_{\beta j}] \sin\left(2\frac{\pi L}{\lambda_{ij}}\right),$$

where $\lambda_{ij} = 2.47$ km$(E/\mathrm{GeV})(\mathrm{eV}^2/\delta_{ij})$ when L is also expressed in km, and $\delta_{ij} = {m_i}^2 - {m_j}^2$. The above expression is given for vacuum. In matter, the probabilities are drastically modified.

Before we specialise to the effects of matter on atmospheric neutrinos and long-baseline neutrinos of interest at ICAL, we list the known central values or bounds on the oscillation parameters obtained from earlier experiments. These values allow us to focus on narrow regions in parameter space and discuss how an ICAL-type4 experiment can further improve the results for some of these parameters, or yield new results on currently unknown parameters.

3.2 Parameter values gleaned from experiments so far

As mentioned earlier, the data indicate that there is very little admixture of the ν_3 mass eigenstate in the flavour state ν_e. In the chosen parametrisation of the mixing matrix, U, this means that θ_{13} is small and the solar neutrino problem can be well-approximated as a 2-flavour (or 2-generation) problem involving only ν_1 and ν_2. Hence the only parameters that appear in the analysis of these (and also the KamLAND reactor) experiments are δ_{21} and θ_{12}. For the same reason, there is only one mass-scale and one mixing angle appearing in the atmospheric neutrino experiments, viz., δ_{32} and θ_{23}. Their values are given below.

Allowed region from Solar + KamLAND results : Assuming CPT invariance, the 3σ allowed range of parameters and the spread (in parenthesis) of δ_{21} and $\sin^2\theta_{12}$ from solar and recent 766.3 day KamLAND data [6] are given by

$$\begin{aligned} 7.2 \times 10^{-5} < \delta_{21} &\equiv \delta_{\mathrm{sol}} < 9.5 \times 10^{-5}\ \mathrm{eV}^2 \quad (14\%)\ ; \\ 0.21 < \sin^2\theta_{12} &\equiv \sin^2\theta_{\mathrm{sol}} < 0.37 \quad (27\%)\ . \end{aligned}$$

The best-fit points are $\delta_{21} = 8.3 \times 10^{-5}$ eV^2 and $\sin^2\theta_{12} = 0.27$.

Atmospheric + accelerator experiments : The allowed range at 3σ of parameters from atmospheric and K2K data [22] is

$$\begin{aligned} 1.4 \times 10^{-3} < |\delta_{32}|/\mathrm{eV}^2 &\equiv \delta_{\mathrm{atm}} < 3.3 \times 10^{-3}\ \mathrm{eV}^2\ ; \\ 0.34 \le \sin^2\theta_{23} &\equiv \sin^2\theta_{\mathrm{atm}} \le 0.66\ . \end{aligned}$$

The best-fit values are $|\delta_{32}| = 2.2 \times 10^{-3}$ eV^2 with $\sin^2\theta_{23} = 0.5$. Whereas δ_{21} is determined to be positive, the sign of δ_{32} is **not** known.

CHOOZ reactor + Atmospheric + Solar + KamLAND experiments [6] : The combined analysis of solar data and the KamLAND and CHOOZ reactor data gives an upper bound on this parameter,

$$\sin^2\theta_{13} \le 0.047 \quad (3\sigma)\ .$$

This bound, which requires a three-flavour analysis, is sensitive to the value of $|\delta_{32}|$ [23].

Parameter	best-fit	3σ
$\delta_{21}/10^{-5}\text{eV}^2$	8.3	7.2 – 9.1
$\lvert\delta_{32}\rvert/10^{-3}\text{eV}^2$	2.2	1.4 – 3.3
$\sin^2\theta_{12}$	0.30	0.23 – 0.38
$\sin^2\theta_{23}$	0.50	0.34 – 0.68
$\sin^2\theta_{13}$	0.00	≤ 0.047

Table 3.1: Best-fit values and 3σ intervals for three flavour neutrino oscillation parameters from global data including solar, atmospheric, reactor (KamLAND and CHOOZ) and accelerator (K2K) experiments.

The allowed range of the (small) mass hierarchy parameter, $\alpha \equiv \delta_{\text{sol}}/\delta_{\text{atm}}$: The bounds on this parameter are,

$$0.024 < \alpha < 0.060 \quad (3\sigma) \ .$$

The best-fit value is $\alpha = 0.035$.

The result of the CHOOZ experiment, which requires the U_{e3} element to be small, plays a key role here. Due to the small value of θ_{13}, the 2-flavour bounds are stable. In Table 3.1 we summarise the results of the global three-neutrino analysis. We use these best-fit values to focus attention on new directions and results with an ICAL detector using atmospheric and long baseline neutrinos as sources.

3.3 Atmospheric Neutrinos

The atmospheric neutrino physics program possible with a magnetised iron tracking calorimeter is substantial. It is possible to observe a clear signal of oscillation by **observing one full oscillation period**. Also the **precision of the parameters,** δ_{32} **and** θ_{23}, can be improved to $\approx 10\%$. A broad L/E range (possible with atmospheric neutrinos) offers the opportunity to probe a large range of δ_{32}. Among the physics capabilities, in addition, are the **sensitivity to matter effects and sign of** δ_{32}. We can also use atmospheric neutrinos to **probe CPT invariance** which is one of the fundamental paradigms of quantum field theories, of which the Standard Model is one.

Atmospheric neutrinos are produced by cosmic ray interactions in the atmosphere, from decays of pions and muons produced in these interactions:

$$\pi \to \mu\nu_\mu \ ; \qquad \mu \to e\overline{\nu}_e\nu_\mu \ .$$

Roughly twice as many muon-type neutrinos (and antineutrinos) are produced as electron-type ones.The flux peaks at zenith angles $\theta_z \sim \pm 90^\circ$, i.e., near the horizon, due to the larger length of atmosphere available in this direction. While the low energy ($E < 1$ GeV) neutrinos have a complicated (θ_z, ϕ) dependence due to various causes including the Earth's magnetic field, they are roughly ϕ-independent at higher energies. Note also that the atmospheric neutrino flux peaks just below a GeV and falls thereafter faster than $1/E^2$. While capturing the low energy flux enhances the event-rate, such events do not contribute significantly to the interesting region where the oscillation is a minimum or a maximum; hence a trade-off between the requirement of higher energy (to enable better detection) and better event rates (to enhance statistics) is required. Typically we assume that ICAL has sensitivity to neutrinos with energy greater than 1 GeV or so.

While the electron-neutrino flux appeared to be as expected, the Super-K collaboration [3] observed that the muon-neutrino events were depleted compared to expectations, with the depletion increasing upto abut 50% in the case of completely up-going neutrinos. Note that the absolute atmospheric neutrino fluxes still have large errors of about 30% on them; the impact of the Super-K data on the neutrino oscillation hypothesis was refined by defining double ratios where these systematic uncertainties could be greatly reduced. Note that the Super-K data does not distinguish the charge of the electrons or muons and so is unable to distinguish neutrino and anti-neutrino events; hence it has no information on matter effects which are different in the two cases.

In short, the zenith angle dependence of muon deficit observed by Super-K could be explained well by neutrino oscillations. Indeed, a recent reanalysis of atmospheric data by the Super-K collaboration disfavours non-oscillation solutions such as neutrino decay or decoherence by more than 3σ. However a direct proof of oscillations, with the observation of both depletion and regeneration of the flux of a given flavour of neutrinos, is still awaited. We demonstrate below that ICAL, with its large range and good resolution in L/E is capable of making such an observation, apart from its ability to observe matter effects.

3.3.1 Observing the oscillation pattern

Apart from their charge discrimination capability, iron calorimeters have a large range in sensitivity to L/E variations compared to water cerenkov detectors and can substantiate the absolute proof of neutrino mass and oscillation already observed by Super-K, via the observation of dips and peaks in the event rate vs. L/E.

In the following, we present the results for L/E sensitivity for such a detector setup. To calculate the event rates in the detector, we assume a two-neutrino oscillation scenario, instead of full three generation exact formulas for survival probabilities. This approximation is quite reasonable in the light of present limits on the mass-square differences from different experiments. While this is sufficient to identify clearly the first dip and extract the values of δ_{32} and $\sin 2\theta_{23}$, disentangling matter effects requires the full three generation calculations.

A useful measure of oscillations is the ratio of up-coming to down-going neutrinos with nadir/zenith angles interchanged. The fluxes of atmospheric neutrinos from directions θ and $(\pi - \theta)$ are expected to be similar in the absence of oscillations, especially for larger energies, $E >$ few GeV. The path-length traversed, L, is related to the zenith angle θ as

$$L = \sqrt{(R + L_0)^2 - (R \sin\theta)^2} - R\cos\theta \ ,$$

where $\theta = 0$ corresponds to neutrinos reaching the detector vertically downwards after traversing a distance L_0 which is the average height above the surface of the earth at which the atmospheric neutrinos are produced. We take this to be about 15 kms, as is the convention. Here R is the radius of the earth.

The replacement $\theta \leftrightarrow (\pi - \theta)$ effectively changes the sign of the second term in the equation above, thus taking, for instance, a down-going neutrino to an up-coming one. The ratio of events in the up-down directions for a given $x = L/E$, therefore, reflects the asymmetry of the up-down fluxes, due to oscillations, and hence is a direct measure of oscillation probability. We define

$$\mathcal{R}(x) = \frac{U}{D}(x) = \frac{\text{No. of events from up-coming muon neutrinos}(x)}{\text{No. of events from down-going muon neutrinos}(\tilde{x})} .$$

In Fig. 3.1, the number of up- and down-going muons (of either sign) in $x = L/E$ bins ($\tilde{x}$ for down-going neutrinos) are presented as solid and broken histograms respectively for two values of δ_{32}, for a mass of 32 ktons. The two histograms are similar in the absence of oscillations. When oscillations are included, the rates for the down-going neutrinos is virtually the same while that for up-coming neutrinos is greatly modified. The dips in L/E bins visible in Fig. 3.1 for the up-going case are the effect of oscillations; the first dip is especially clear.

Fig. 3.2, shows, for the same values of δ_{32}, the ratio $\mathcal{R}$ of up to down going muons in the detector, along with assumed $\sqrt{N}$ errors. Note that such a ratio eliminates [39] the large systematic errors in the normalisation of the atmospheric neutrino flux, which may be as large as 30%. Since the down-going neutrino event rate is hardly affected by oscillations, we expect $\mathcal{R}$ to be a measure of the ν_μ survival probability, $P_{\mu\mu}$, smeared, however, by the finite detector resolution:

$$P_{\mu\mu} = 1 - \frac{\sin^2(2\theta_{23})}{2} \left[1 - R \cos(2.54\, \delta_{32} L/E)\right] , \tag{3.2}$$

where the resolution function R is a Lorentzian in L/E with width $\sigma = 50\% L/E$.

The position of the dip in the observable $\mathcal{R}$ is thus a measure of δ_{32} while the *value* of this observable at the minimum is a measure of θ_{23}. The solid line is the best fit to the formula Eq. 3.2. It is clear that the dip and subsequent rise in this quantity should yield firm evidence of oscillations within a few years of data-taking. It is evident that poor resolutions decrease the sensitivity to θ_{23}.

Recall that the spread in δ_{32} is 39% from the Super-K zenith data whereas it is 22% from the Super-K L/E data. Thus with L/E data one gets an improved precision in the measurement of δ_{32}. Hence a good experimental resolution in L/E is extremely important for an accurate determination of both δ_{32} and θ_{13}. The range of $\sin^2\theta_{23}$ however is unaffected: $\delta(\sin^2\theta_{23}) \sim 5\%$. Atmospheric neutrinos and a large magnetised iron calorimeter like MONOLITH, INO [13, 19] can improve the precision of both the atmospheric oscillation parameters.

Fig. 3.2 (right), shown here as a check on the calculations, gives the 68%, 90% and 99% CL contours obtained from fitting the ratio $\mathcal{R}$ to $P_{\mu\mu}$ as given in Eq. 3.2, and shows the best-fit parameter values for δ_{32} and $\sin^2 2\theta_{23}$ returned by MINUIT, which compare very well with our input parameters and indicate a 10% sensitivity on the oscillation parameters.

3.3.2 Matter effects in atmospheric μ^-/μ^+ events

The number of muons observed at ICAL with atmospheric neutrinos as source depends on $P_{\mu\mu}$ and $P_{e\mu}$, which are the probabilities of survival of ν_μ and conversion of a $\nu_e \to \nu_\mu$ respectively. These in turn depend on the energy and path-length E and L of the neutrino. We focus on energy and path length ranges where matter effects are very large. The expected event rates for μ^- and μ^+ in ICAL were computed using Bartol flux[1] tables [24], a modest

[1] It is expected that the results will not be sensitive to whether Honda [25] or Bartol flux tables are used as long as the ratios of events are involved.

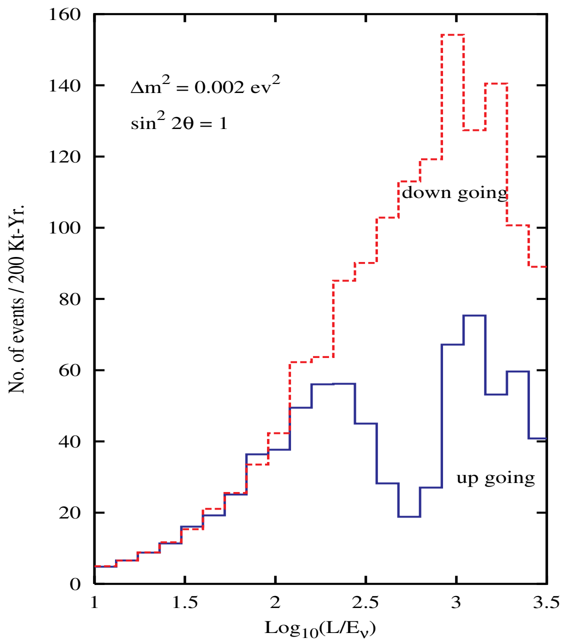

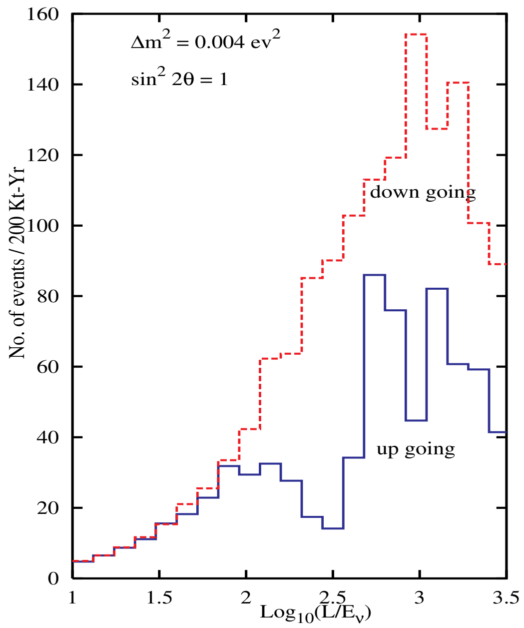

Figure 3.1: The number of up- (solid histogram) and down-going (broken histogram) muons (of either sign) in L/E bins are presented for two values of $\delta_{32} = 0.002,\ 0.004$ eV^2 for an exposure of 160 kton-years at ICAL.

muon identification efficiency of 50% and an exposure time of 1000 kton-years. The event rates are calculated for the E range 5–10 GeV and L range 6000–9700 km. The distribution of the event rates, both in the case of vacuum and matter oscillations are shown in Fig. 3.3 as a function of L and L/E respectively for $\delta_{32} > 0$, with $|\delta_{32}| = 2\times10^{-3}$ eV^2 and $\sin^2 2\theta_{13} = 0.1$, well within the allowed limits of these parameters.

The total number of μ^+ events in the case of vacuum oscillations is 105 which changes to 103 on inclusion of matter effects. The total number of μ^- events, on the other hand, is 261 in the case of vacuum oscillations and this reduces to 204 on inclusion of matter effects. The distribution of the event rates, both in the case of vacuum and matter oscillations, is shown in Fig. 3.4 as a function of L and L/E for the inverted hierarchy when $\delta_{32} < 0$. A comparison with Fig. 3.3 immediately shows the impact of hierarchy on the distribution of events when matter effects are included. Since matter effects are *always* present for the large path lengths under consideration, a clear distinction between the direct and inverted mass hierarchy is possible.

We thus have a 4σ signal for matter effects for neutrino parameters $\delta_{32} = 0.002$ eV^2 and $\sin^2 2\theta_{13} = 0.1$. We estimate that the matter effect leads to about 2.5σ signal for the same δ_{32} and a reduced $\sin^2 2\theta_{13} = 0.05$. A systematic study of sensitivity of magnetised iron detectors to matter effects as a function of θ_{13} and δ_{32} is underway.

The event rates shown in Figs. 3.3 and 3.4 can have large systematic errors arising from uncertainties in the flux normalisation. This can be largely removed by defining a generalisation of the usual up by down events ratio. In particular, the distinction (and hence measurement possibilities) between the two hierarchies can be amplified by defining

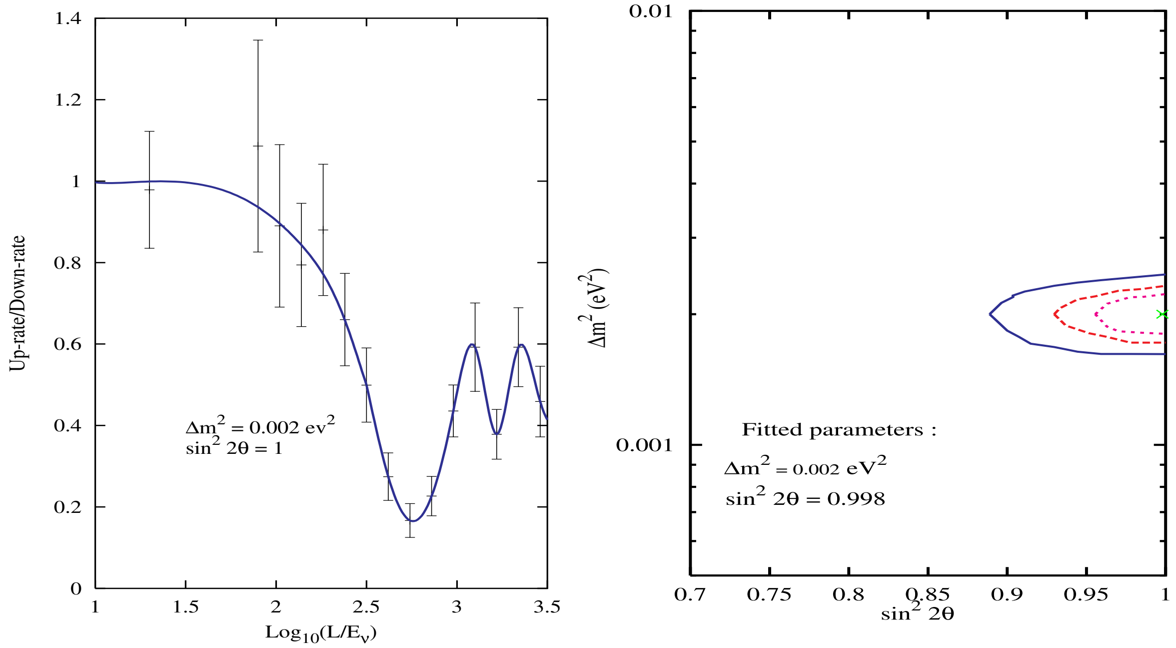

Figure 3.2: Left: The ratio of up to down muon events shown in Fig. 3.1 along with the statistical error bars plotted against $\log_{10} L/E$. The solid line is the best-fit curve. Right: The 68%, 90% and 99% CL contours obtained from the fits with the cross depicting the best-fit parameter values in δ_{32} and $\sin^2 2\theta_{23}$ parameter space.

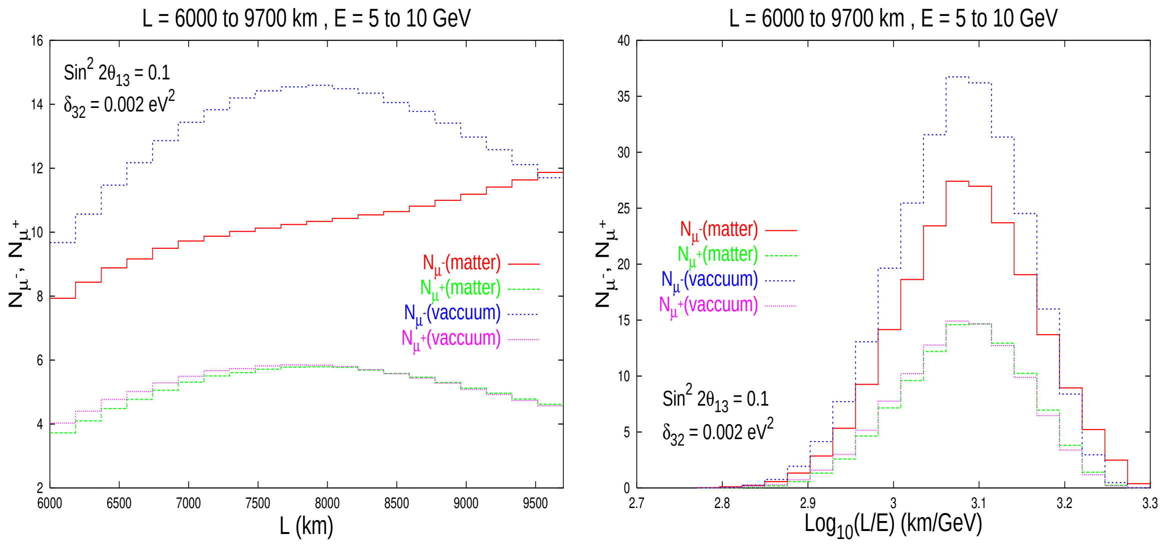

Figure 3.3: Left: The total event rate for muons and anti-muons in matter and in vacuum plotted against L. Right: The total event rate for muons and anti-muons in matter and in vacuum plotted against $\log_{10} L/E$ for a restricted range of L and E.

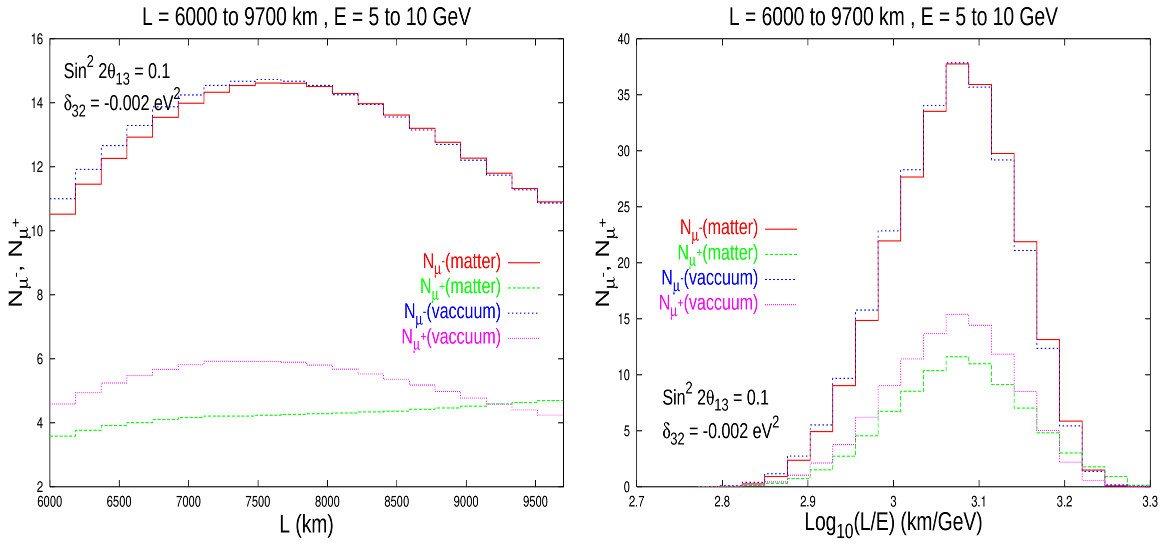

Figure 3.4: Same as Fig. 3.3 for inverted hierarchy: $\delta_{32} = -0.002$ eV^2.

the difference asymmetry,

$$\mathcal{A}_N(x) = \frac{U}{D}(x) - \frac{\overline{U}}{\overline{D}}(x) \ , \tag{3.3}$$

where $x = L/E$, $\overline{U}(U)$ denotes the up-going muon (anti)neutrino event rate and $\overline{D}(D)$ the corresponding down-going rate.

The asymmetry, calculated numerically, and integrated over $E_{\rm min} > 4$ GeV, is plotted as a function of L/E in Fig. 3.5 for $|\delta_{32}| = 1, 2, 3 \times 10^{-3}$ eV^2. The thick (blue) curves in the figure correspond to the direct mass hierarchy (labelled D) and the thin (red) curves to the inverted mass hierarchy (labelled I). The curves in each envelope correspond to $\theta_{13} = 5, 7, 9, 11$ degrees ($\sin^2 2\theta_{13}$ from 0.03–0.14) with the asymmetry increasing symmetrically with θ_{13} about the $\mathcal{A}_N = 0$ line for direct and inverted hierarchies. All other relevant oscillation parameters are kept fixed to their best-fit values. It is seen that the direct and inverted asymmetries are exactly out of phase. The maximum divergence between the direct and inverted hierarchies is smaller in the first envelope than in the second; these correspond to the first dip and rise in the up/down events ratio.

Detailed analysis shows that the set of measurements required for resolving the hierarchy problem may need about 1000 kton-years of exposure given the resolution in energy and zenith angle available at present provided $\theta_{13} > 6°$. With better resolution for both energy and direction, it may be possible to bring the exposure down to about 500 kton-years. Detailed calculations are in progress.

3.3.3 Discrimination between $\nu_\mu \to \nu_\tau$ and $\nu_\mu \to \nu_s$

The ICAL detector also provides a new way of distinguishing whether the muon neutrino deficit observed by previous experiments is due to oscillations of muon neutrinos to other active flavours (predominantly $\nu_t au$) or to sterile ones. If the dominant oscillation is $\nu_\mu \to \nu_\tau$,

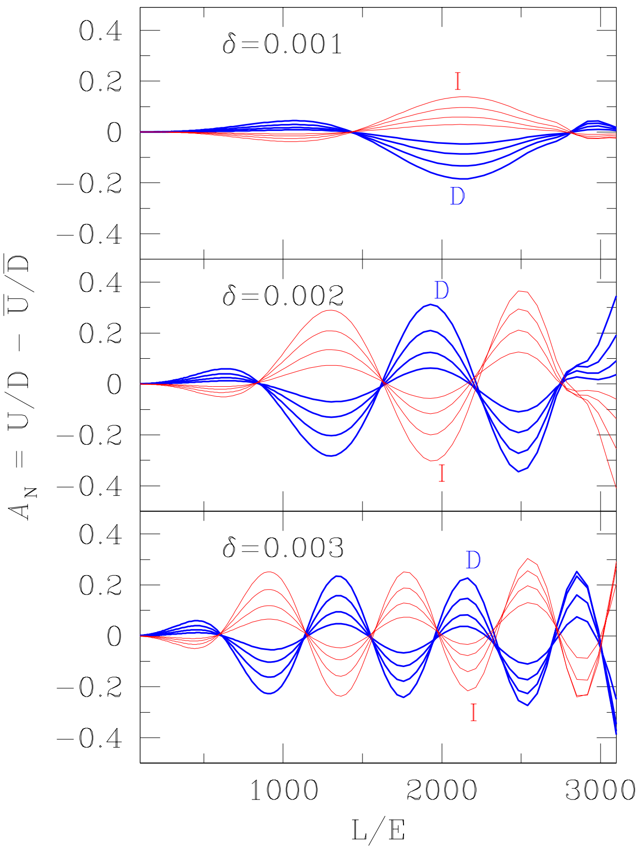

Figure 3.5: The difference asymmetry (difference of up/down ratios of muon neutrinos and antineutrinos) as a function of L/E for $E > 4$ GeV. The three panels correspond to $\delta \equiv |\delta_{32}| = 1, 2, 3 \times 10^{-3}$ eV^2. The thick (blue) curves correspond to the direct $\delta_{32} > 0$ and the thin (red) curves correspond to the inverse $\delta_{32} < 0$ hierarchy. The innermost curve in each envelope corresponds to $\theta_{13} = 5°$ and the outermost corresponds to $\theta_{13} = 11°$ with 7° and 9° in between. For other parameters the best fit values given in the text are chosen.

as appears probable from the Super-K data, there should be charged current (CC) production of τ leptons in the detector, originating from the ν_τ produced due to these oscillations. At these energies, the τ lepton decays very rapidly, and roughly 80% of the time this decay does *not* produce a muon. The visible hadronic activity generated in these events has the appearance (if specific cuts for τ detection are not designed) of a neutral-current (NC) event due to the lack of a visible charged lepton track.

Thus this oscillation scenario has a significantly different up/down ratio of "muon-less" events when compared to the $\nu_\mu \to \nu_s$ possibility. In fact, the asymmetry in the ratio assumes positive values in one case ($\nu_\mu \to \nu_\tau$) and negative values in the other ($\nu_\mu \to \nu_s$), since the upward rate is enhanced significantly by CC τ events (which appear as "fake" NC events) in the former case, but depleted if the oscillation is to sterile neutrinos since they will have neither CC nor NC interactions.

Fig. 3.6 quantifies this, where we show the ratio of the asymmetry in the rates for two different values of δ_{32}, for both possible modes of oscillation. Note also the relative difference visible for both these values, showing that this provides an independent handle on the value of this parameter, in addition to the sensitivity discussed in the CC mode above.

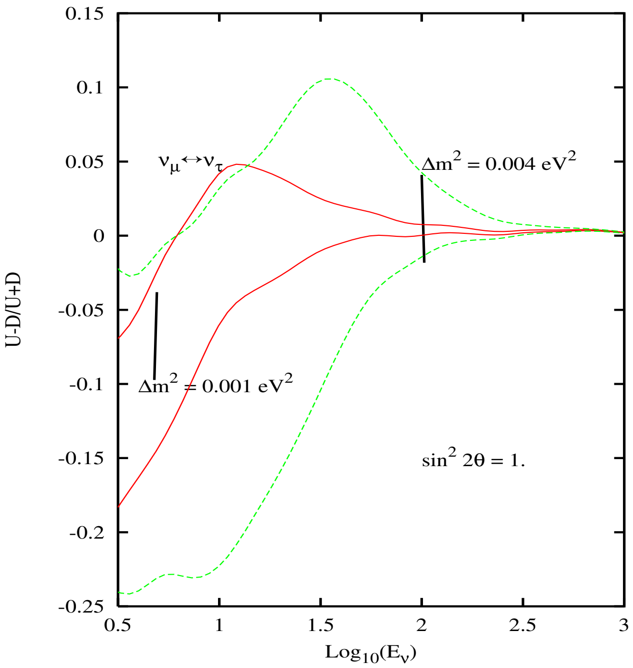

Figure 3.6: Ratio of the asymmetry of muon-less events plotted as a function of the energy $\log_{10}(E/\mathrm{GeV})$ for different values of δ_{32}, for both possible modes of oscillation, $\nu_m u \to \nu_\tau$ and $\nu_\mu \to \nu_s$. The solid (dotted) lines correspond to $\delta_{32} = (1)4 \times 10^{-3}$ eV^2. Oscillation into steriles result in a more negative asymmetry at small energies.

3.3.4 Probing CPT Violation

It has been proposed that the atmospheric neutrinos in conjunction with ICAL may also be used as a probe of the level of Lorentz and CPT violation [27]. The survival probabilities for neutrinos and antineutrinos, in a two flavour scenario, are identical. However in the presence of the effective C- and CPT-odd interaction terms $\bar{\nu}_L^\alpha b^\mu_{\alpha\beta}\gamma_\mu \nu_L^\beta$, where α and β are flavour indices, the expression for the survival probability is

$$P_{\mu\mu}(L,E) = 1 - \sin^2 2\theta \ \sin^2\left[\left(\frac{\delta_{32}}{4E} + \frac{\delta b}{2}\right) L\right] \ , \tag{3.4}$$

where δ_{32} and δb are the differences between the eigenvalues of the mass matrix m^2 and the interaction matrix b, respectively. Note that δb has units of energy (GeV). Observable CPT violation in the 2-flavour case is a consequence of the interference of the CPT-even and CPT-odd terms. We focus on the survival probabilities for ν_μ and $\bar{\nu}_\mu$ which are a measure of these violations. Thus one can define an asymmetry,

$$\Delta P^{\mathrm{CPT}}_{\mu\mu} = P_{\mu\mu} - P_{\bar{\mu}\bar{\mu}} = -\sin^2 2\theta \, \sin\left(\frac{\delta_{32} L}{2E}\right) \sin \delta b L \ . \tag{3.5}$$

In Fig. 3.7, we plot the ratio of muon to anti-muon events vs. the path length L using the Bartol atmospheric neutrino flux. We show that (by studying the variation with L), it is possible to detect the *presence* and also obtain a *measure of the magnitude* of δb by studying the minima and zeros for $\delta b \geq 3 \times 10^{-22}$ GeV. For some-what lower values of δb

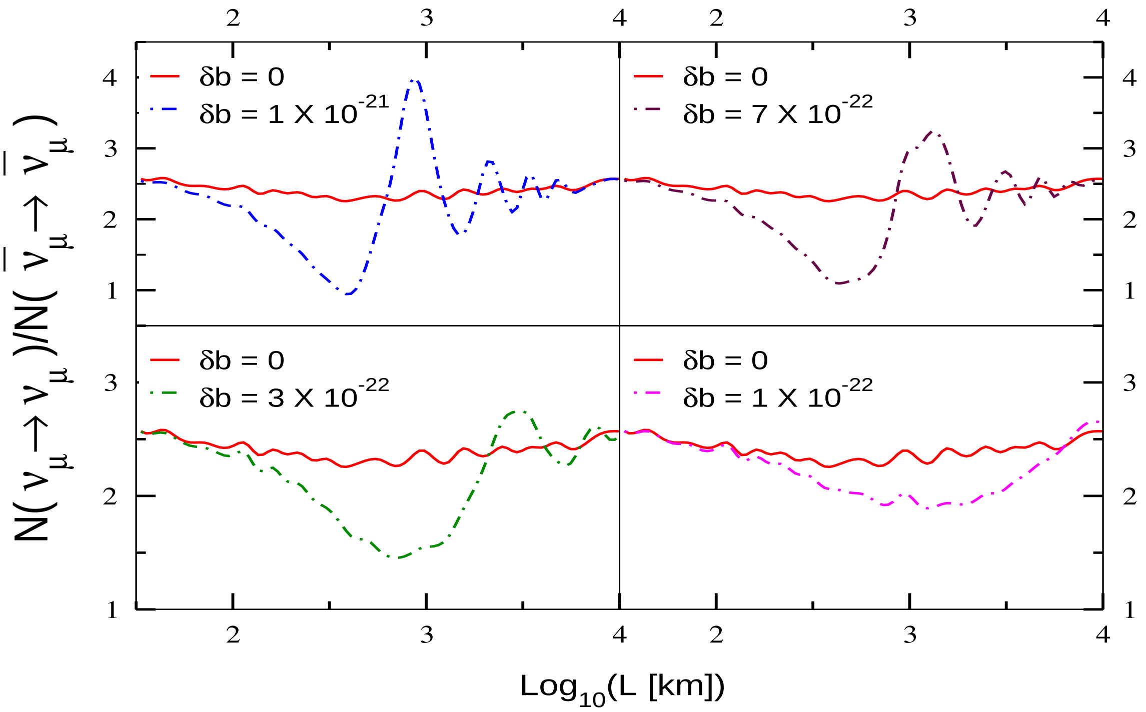

Figure 3.7: The ratio of total (up+down) muon to anti-muon events plotted against $\log_{10} L$ for different values of δb (in GeV). The oscillation parameters used in all the plots $\delta_{32} = 2 \times 10^{-3}$ eV^2 and $\sin^2 2\theta_{23} = 1$.

(but $\geq 3 \times 10^{-23}$ GeV), the plots vs. L/E indicate only the *presence* of CPT violation, without the same discriminating capability. The bounds that we have obtained compare very favourably with those obtained from neutrino factories [28]. We note that the value of δb compares with $\delta_{32}/2E \approx 10^{-21}$ GeV. Our calculations indicate that an exposure of 400 kton-year would be sufficient for statistically significant signals to emerge.

3.3.5 Constraining long-range leptonic forces

Long range forces in the context of particle physics originated with the ideas of Yang and Lee and Okun [29] who proposed that gauging the baryon number or lepton number would give rise to a composition-dependent long-range force which could be tested in the classic Eotvos-type experiments. A special class of long-range forces which distinguish between leptonic flavours have far-reaching implications for neutrino oscillations which may be used as a probe of such forces.

The leptonic long-range forces which distinguish between their flavours have been shown to significantly influence the oscillations of the atmospheric, solar as well as terrestrial neutrinos. The potential generated by these forces distinguishes between neutrinos and anti neutrinos. Thus the magnetised iron calorimeter, ICAL, which can distinguish the charge of the muons, can provide more sensitive tests of these forces. Detailed analysis in the case of atmospheric neutrinos shows that such detectors have the potential to further improve bounds on the long range couplings by an order of magnitude [30].

3.4 Neutrino Factories

The possibility of neutrino beams from muon storage rings has received a lot of attention in the recent literature [31]. Such facilities provide intense, controlled, high luminosity neutrino beams that are almost pure $\nu_\mu + \bar{\nu_e}$ or $\nu_e + \bar{\nu_\mu}$ depending on the sign of the stored muon. With its charge discrimination capability, a magnetised iron calorimeter offers unique capabilities to exploit the physics potential of such sources. Such a possibility, it must be remembered, is still some way into the future and affords the option of exhausting the potential of ICAL as a detector of atmospheric neutrinos before it is switched into the long baseline mode.

As is well understood by now, these kind of high purity, high intensity neutrino beams may provide the best and cleanest, if not the only, way to achieve at least three goals mentioned above, viz., determining the neutrino mass hierarchy, θ_{13}, and the CP phase δ. While the determination of mass hierarchy seems to be rather straight forward, subject to constraints on the magnitude of θ_{13}, determination of θ_{13} and δ are sensitive to the combination of baseline and detector chosen. Many neutrino factory locations and corresponding end-detector sites are under consideration and active discussion all around the world. In what follows, we explore the physics discovery potential of ICAL at INO, when used as an end-detector for a neutrino factory beam originating from the Japan Hadron Facility at Jaeri (JHF) and another from Fermilab, USA. There are two possible locations in India. One is at *PUSHEP* in the southern part of India. The other one is at *Rammam* in the north-eastern part. We will consider in the following the four possible baseline lengths corresponding to these sites: *JHF–Rammam*: 4865 km; *JHF–PUSHEP*: 6591 km; *Fermilab–Rammam*: 10489 km and *Fermilab–PUSHEP*: 11296 km. A schematic of the baselines is shown in Fig. 3.8.

3.4.1 Determination of θ_{13}

We first explore the reach for θ_{13}. Recall that the CHOOZ bound on this parameter is $\sin^2 2\theta_{13} < 0.149$ (3σ). This is the driving parameter for $\nu_e \to \nu_\mu$ oscillations, and for CP violation searches. We stress that this is true with or without matter effects. The next generation of experiments will thus have the determination of θ_{13} as one of the primary goals.

The key to determining θ_{13} from long baseline experiments is to establish the *sign* of the detected muon. For example, when teh beam components are ν_e and $\overline{\nu}_\mu$, μ^+ are expected to be detected in the absence of oscillations. However, $\nu_e \to \nu_\mu$ conversion is possible in the presence of oscillations, whence μ^- may be detected instead. This is known as the wrong-sign muon signal. Since backgrounds are very low at neutrino factories, a few such events signal oscillations unambiguously.

Fig. 3.9 demonstrates the achievable values of $\sin\theta_{13}$ as a function of the muon detection threshold energy E_μ^{th} of the detector. The reach is determined as the value which is necessary to collect 10 signal events (that is events that involve wrong sign muons) for a given kton-year exposure. We show the reach capabilities for an entry-level configuration ($E_\mu^{beam} = 20$ GeV, 10^{19} decays per year). For a median detector size of 50 ktons running for 1 year, at a muon detection threshold of 2 GeV, the reach corresponds to $\sin\theta_{13} = 0.038$ or $\sin^2 2\theta_{13} = 0.0057$ for *Rammam* and a slightly worse value for *PUSHEP*, as shown. The reach values improve to $\sin\theta_{13} = 0.026$ or $\sin^2 2\theta_{13} = 0.0027$ for *Rammam* if the energy of the beam is increased to 50 GeV, keeping other variables the same as before. In all of the above, the "passive" parameters $\delta_{32}, \delta_{21}, \sin^2 2\theta_{23}$ and $\sin^2 2\theta_{12}$ are held to their (best-fit) values specified above.

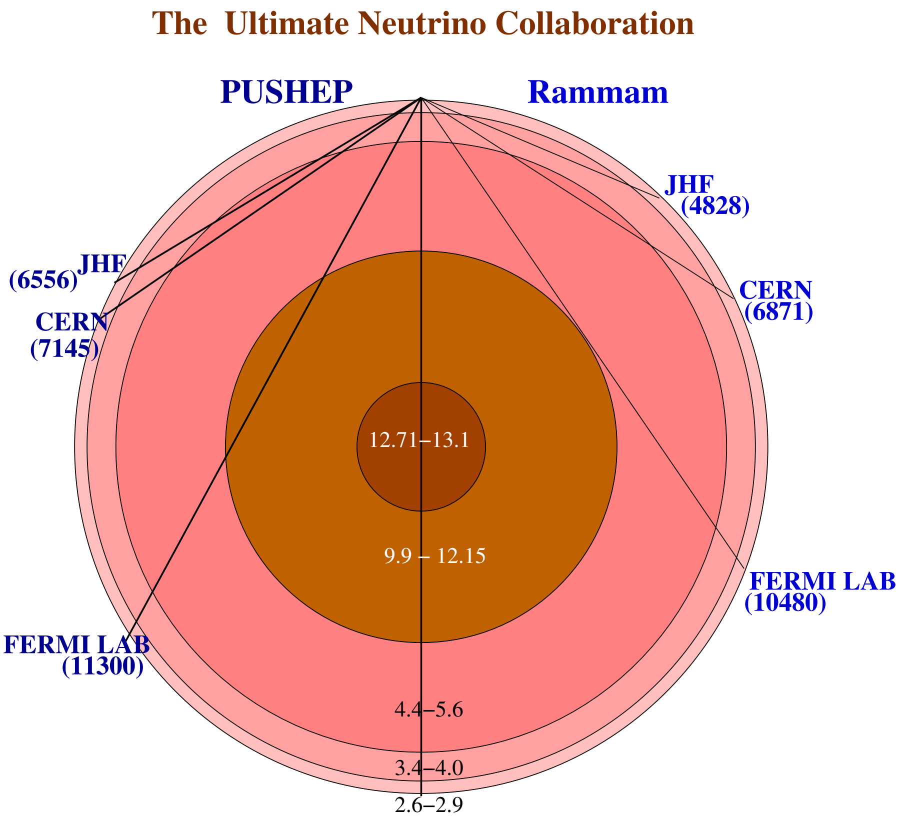

Figure 3.8: Baselengths (in kms) from the proposed neutrino factories to the two proposed INO sites in India. The left half shows the baselengths to the site at PUSHEP whereas the right-half shows the baselengths to the site at Rammam. The densities of the layers that the neutrinos pass through are also indicated. Note that the CERN–PUSHEP baseline is near "magic".

A second method of obtaining a measure of θ_{13} is via matter effects which show up once the baselines are long. In particular, the total right-sign muon rate varies measurably with θ_{13}, as demonstrated in Fig. 3.10 for the *JHF-PUSHEP* baseline. Here the number of such events are shown as a function of E_ν/δ_{32} for a neutrino factory with 10^{21} muon decays/yr. Clearly, a measure of this important parameter, even if it is small, is possible via this method. Note that the event-rate peaks nicely for neutrinos in the 10–20 GeV range for the currently allowed and favoured range of values of δ_{32} from atmospheric neutrino data.

3.4.2 Sign of δ_{32}

We next examine the capability to determine the sign of E_ν/δ_{32} that these baselines offer. This is sensitive once again to the wrong-sign muon rate generated by $\nu_e \to \nu_\mu$ oscillations. For small θ_{13}, if the matter potential has the same sign as δ_{32}, then $A/\delta_{32} \propto\sim E_\nu/\delta_{32} > 0$, and matter effects lead to an enhancement of $\nu_e \to \nu_\mu$ and a suppression of $\bar{\nu_e} \to \bar{\nu_\mu}$. The converse is true if the sign of A/δ_{32} is reversed.

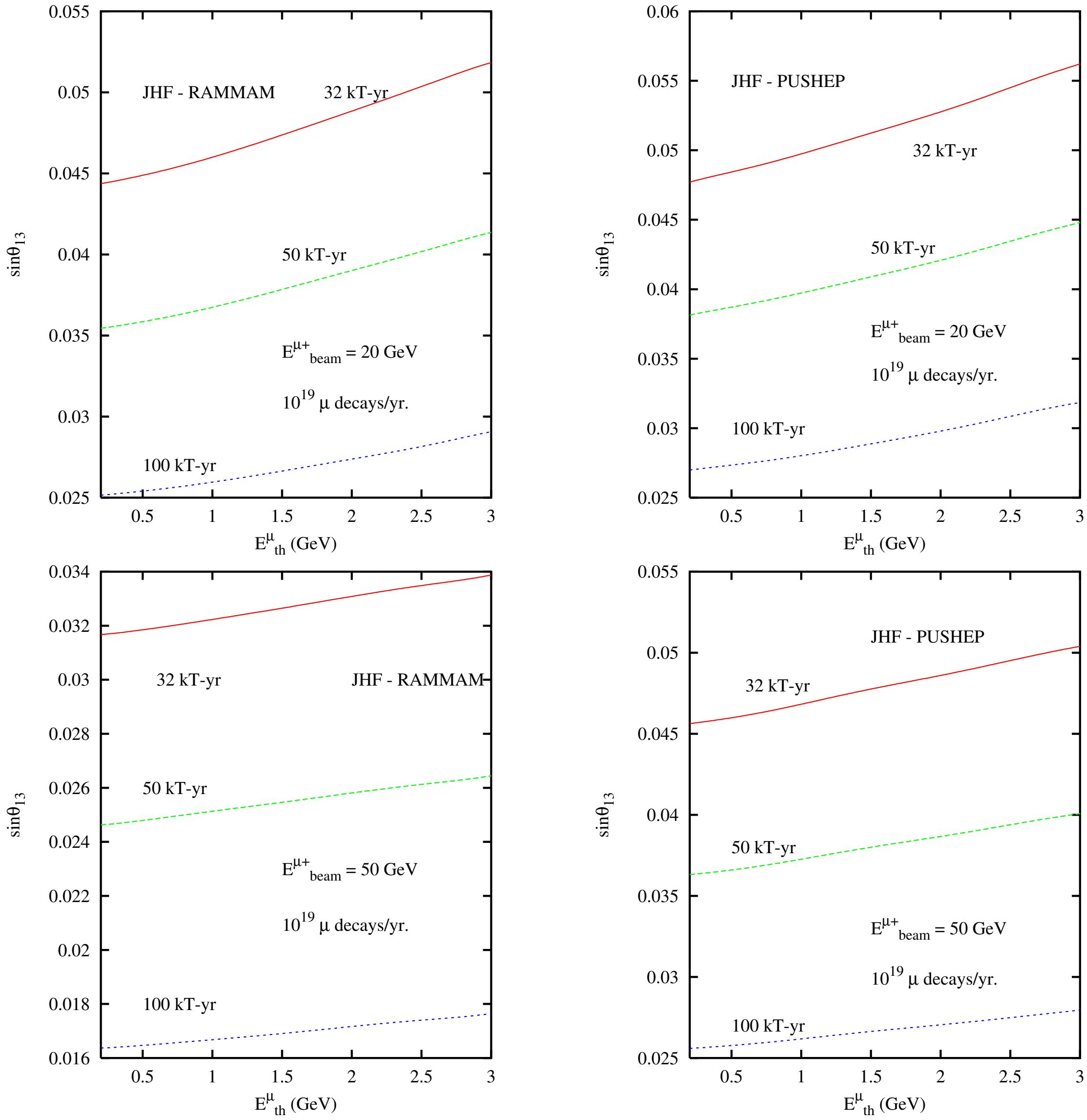

Figure 3.9: The $\sin\theta_{13}$ reach for detector exposures of 32 kton-year, 50 kton-year and 100 kton-year for an entry-level neutrino factory configuration with $E_\mu^{beam} = 20$ GeV for the JHF-Rammam and the JHF-PUSHEP baseline. The lower panels show the change in reach if the storage muon energy is increased to 50 GeV, keeping the number of decays per year the same, i.e, 10^{19}/yr; there is substantial improvement in the reach in the case of the JHF-Rammam baseline.

Fig. 3.11 shows the sign discrimination capability for an entry-level neutrino factory configuration with a 32 kton detector running for a year. For both the *Rammam* and *PUSHEP* baselines, the sign dependent difference in event rates is easily measurable in terms of wrong sign muon events. For comparison, we also show the difference in event-rates for a JHF-China baseline (1952 km) were a similar detector to be set up there. Fig. 3.12 shows the improvement (or rather, the overkill) possible with an upgraded factory yielding 10^{21} decays per year with a beam energy of 50 GeV running for one year, with the detector mass increased to 50 kton. Clearly, the long baseline experiments (even with modest goals) can achieve in one year of data-taking what may require a decade to accomplish with an atmospheric neutrino programme.

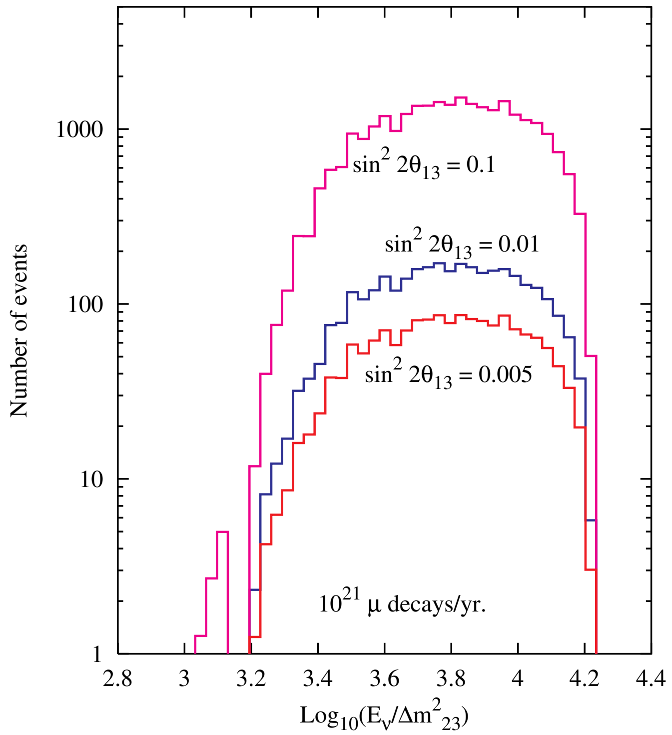

Figure 3.10: The number of right-sign muon events as a function of E_ν/δ_{32} (GeV/eV^2) for the JHF-PUSHEP baseline. The dip to the left of the distribution is due to a minimum of the oscillation probability.

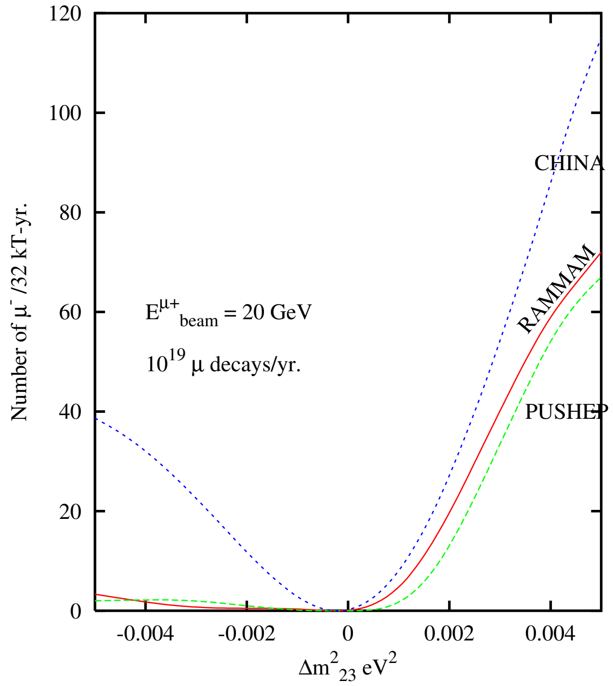

Figure 3.11: The number of wrong-sign muon events as a function of δ_{32} for the three baselines from JHF, demonstrating the sign discriminating capability which arises as a result of matter effects. Event rates are computed for an entry-level configuration with a 32 kton-year exposure, beam energy of 20 GeV and 10^{19} decays per year.

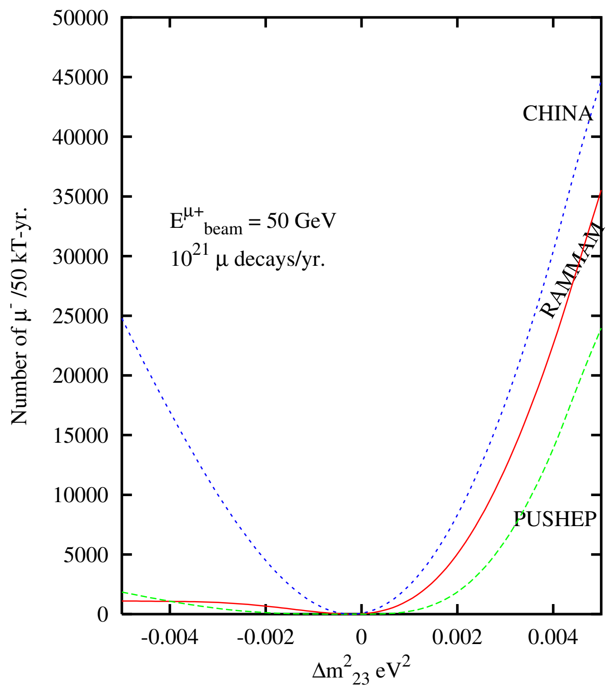

Figure 3.12: The same as Fig. 3.11, but for an upgraded neutrino factory configuration with a 50 kton-year exposure, 10^{21} decays per year and a beam energy of 50 GeV.

3.4.3 Probing CP violation in leptonic sector

We next examine the discovery potential for what many consider as the primary open issue in the lepton sector, i.e., the presence or absence of CP violation. In the standard three generation scenario, this is parametrised by a single phase δ in the lepton mixing matrix. In principle, rates for particles and their CP conjugates exhibit a difference stemming from terms proportional to $\sin\delta$ in the oscillation probability. Generally, these differences are small and difficult to disentangle from matter oscillation effects, which in long baseline situations dominate differences due to CP. The detectability depends sensitively on $\sin^2 2\theta_{13}$, δ_{21}, the energy and baseline, among other parameters, besides of course on the magnitude of $\sin\delta$. In particular, studies of CP violation in the long baseline mode is possible only if θ_{13} is not zero.

One possible signature is the ratio of wrong-sign muon events for equal exposures when the neutrino factory runs with muons and anti-muons stored in the ring in turn. Thus for negatively charged stored muons, one expects $\bar{\nu_e} \to \bar{\nu_\mu}$ oscillations to produce CC induced positively charged muons, and vice-versa for a run with stored μ^+ in the ring.

In Fig. 3.13 we show (as a function of baseline length) the ratio of wrong-sign muon events for a run with negatively charged muons in the storage ring (and, hence, the resultant μ^+ events due to oscillations, denoted by $N(\mu^+)$) to that for a run with positively charged muons (yielding μ^- events via oscillations, denoted by $N(\mu^-)$). The calculations are performed for a factory with a beam energy of 20 or 50 GeV and a muon decay yield of 10^{21} decays per year. In the top left panel, a value of $\sin\theta_{13} = 0.1$ ($\sin^2 2\theta_{13} = 0.04$) has been assumed, along with a run of 1 year each of either sign of stored muon, and a detector mass of 32 kton. Note that the antineutrino cross-sections are about a factor of two smaller than the neutrino cross-sections. The dashed curves are for $\delta = \pm\pi/2$ and the data points show the values (along with statistical errors) for no CP violation ($\delta = 0$) for the Beijing, *Rammam*

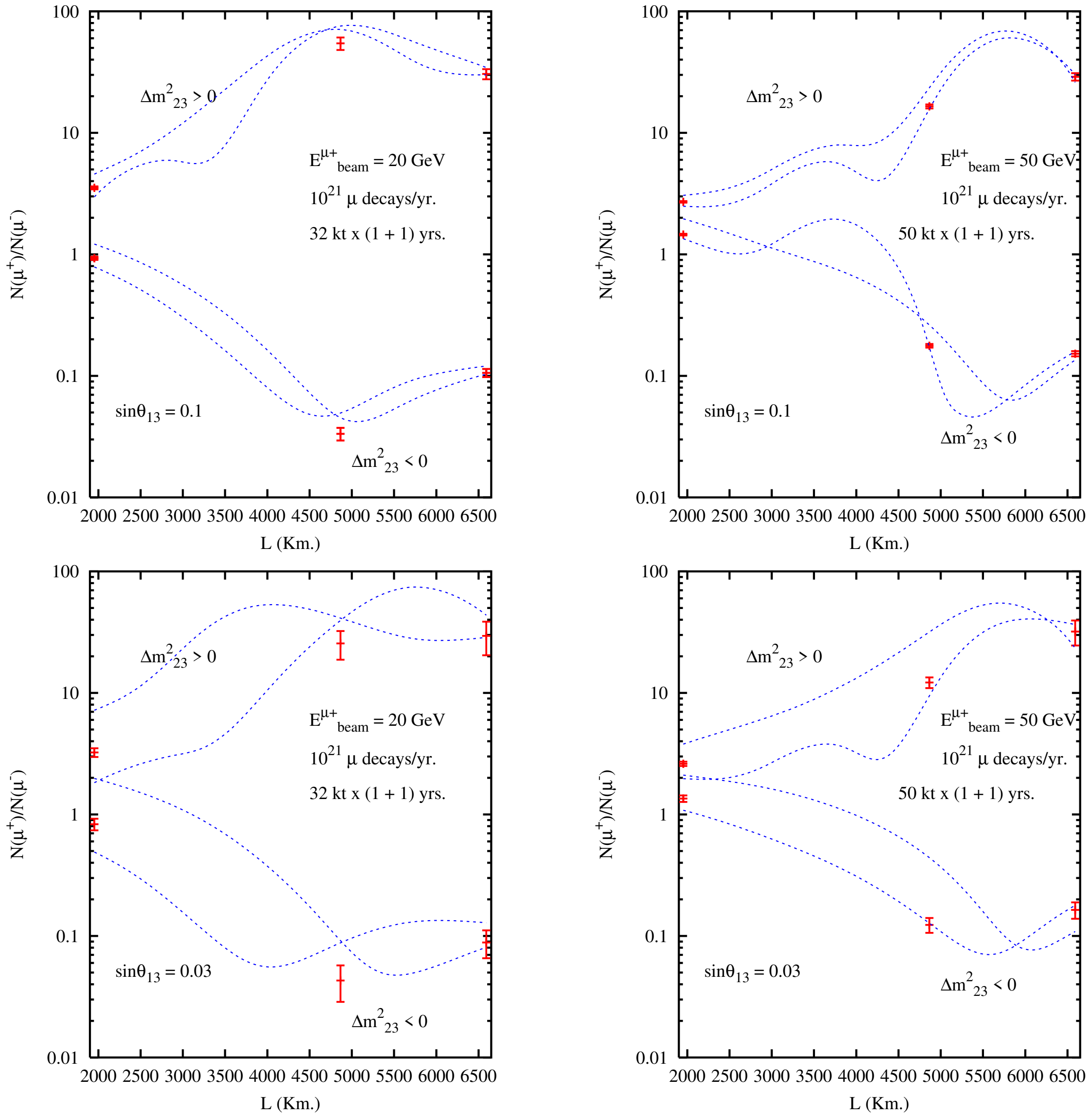

Figure 3.13: The ratio of wrong-sign muon events for equal-time runs of opposite sign muons and $\delta = \pm\pi/2$ (dashed curves) and $\delta = 0$ (data points, with statistical errorbars) in the storage ring, versus baselength. The top row shows the results for $\sin\theta_{13} = 0.1$ ($\sin^2 2\theta_{13} = 0.04$) and 10^{21} decays per year, with beam energies of 20 GeV in one case and 50 GeV in the other. The bottom row shows the results when $\sin\theta_{13} = 0.03$ ($\sin^2 2\theta_{13} = 0.0036$). The positions of the data points reflect the baselengths for detector locations at Beijing, Rammam and PUSHEP in order of increasing length.

and *PUSHEP* baselines respectively.

The two sets of curves (upper and lower) correspond to opposite signs of δ_{32}, which reflect the effects of matter. We note that CP effects tend to cancel (i.e., are small) for this configuration at *PUSHEP*; hence the measurements there afford an opportunity to effectively isolate and measure the matter effects. Such measurements can be used in conjunction with measurements at a baseline where CP effects are relatively large and afford a cleaner discrimination between $\delta = 0$ and a non-zero value of this parameter. This is exemplified in the top right panel of Fig. 3.13 which uses a higher beam energy of 50 GeV and a slightly more massive detector of 50 ktons.

The Rammam baseline offers an opportunity to detect the presence of a δ which is different from zero, especially as exposure (in kton-year) and statistics improve. The bottom panels of Fig. 3.13 show the CP capabilities for the same two configurations but for a lower value of $\sin\theta_{13}$, namely 0.03. Note that both our chosen values of this parameter are well below the current CHOOZ bound. The conclusions for both *Rammam* and *PUSHEP* are similar to the ones above. The former provides us with an opportunity to measure the presence of a non-zero CP violation, while the latter provides us an opportunity to separate matter effects from the CP violation contributions in conjunction with another long-baseline experiment.

We note that cleaner CP measurements are possible with other kinds of detector, in particular, those that are capable of both electron and mu detection, or, even better, tau detection. However, while offering excellent possibilities for determining $\sin\theta_{13}$ down to very small values, as well as establishing the neutrino mass hierarchy, the wrong-sign muon technique probes the CP phase as well.

Finally in Fig. 3.14, we present the CP capabilities for baselengths corresponding to that from Fermilab to *PUSHEP* and *Rammam*. The input parameters remain the same as in Fig. 3.13. For comparison we have presented the same numbers for the baselines corresponding to JHF-*Rammam* and JHF-*PUSHEP* again.

3.4.4 Detecting Large Matter Effects in $\nu_\mu \rightarrow \nu_\tau$ Oscillations

The $\nu_\mu \rightarrow \nu_\tau$ oscillation probability $P_{\mu\tau}$ can also undergo significant change (a reduction as high as $\sim 70\%$ or an increase of $\sim 15\%$) compared to its vacuum values over an observably broad band in energies and baselines due to matter effects. The maximal effect in $\nu_\mu \rightarrow \nu_\tau$ oscillations occurs at $L \sim 9700$ km, 9300 km, 9900 km for $\sin^2 2\theta_{13} = 0.05$, 0.1 and 0.2 respectively. This can also induce appreciable changes in the muon neutrino survival probability $P_{\mu\mu}$ in matter [32]. For $\nu_\mu \rightarrow \nu_\mu$, the effect is maximal at 7000 km for $\sin^2 2\theta_{13} = 0.1$.

The τ appearance rate as a signal for matter effects can also be searched for in special τ detectors being thought of for neutrino factories. Similarly, detectors capable of measuring muon survival rates [33], such as ICAL can detect the effects visible in the bottom panels of Fig. 3.15 at neutrino factories. Typical baselines from existing and proposed neutrino factories to two possible sites in India for INO include $L \sim 7000$ km (*CERN-PUSHEP* and *CERN-Rammam*). Also baselines $L \sim 10500$ km are possible (for *Fermilab-PUSHEP* and *Fermilab-Rammam*) and these are well within the range of baselines where these effects are large and observable. Detailed calculations are in progress.

3.5 Other physics possibilities

Kolar events : Earlier experiments at KGF had recorded unusual events [17] indicating the possibility of a long-lived particle with a large production rate. This phenomenon is as yet not well understood. The proposed detector ICAL at INO will be capable of observing many more such events leading to a better understanding and possibly clarifying the origin of these unusual events. We discuss these events briefly below.

In the neutrino experiments at 7000 MWE, as well as those conducted later at 3375 MWE and the proton decay experiments in KGF mines, it was noticed that some multi-track events

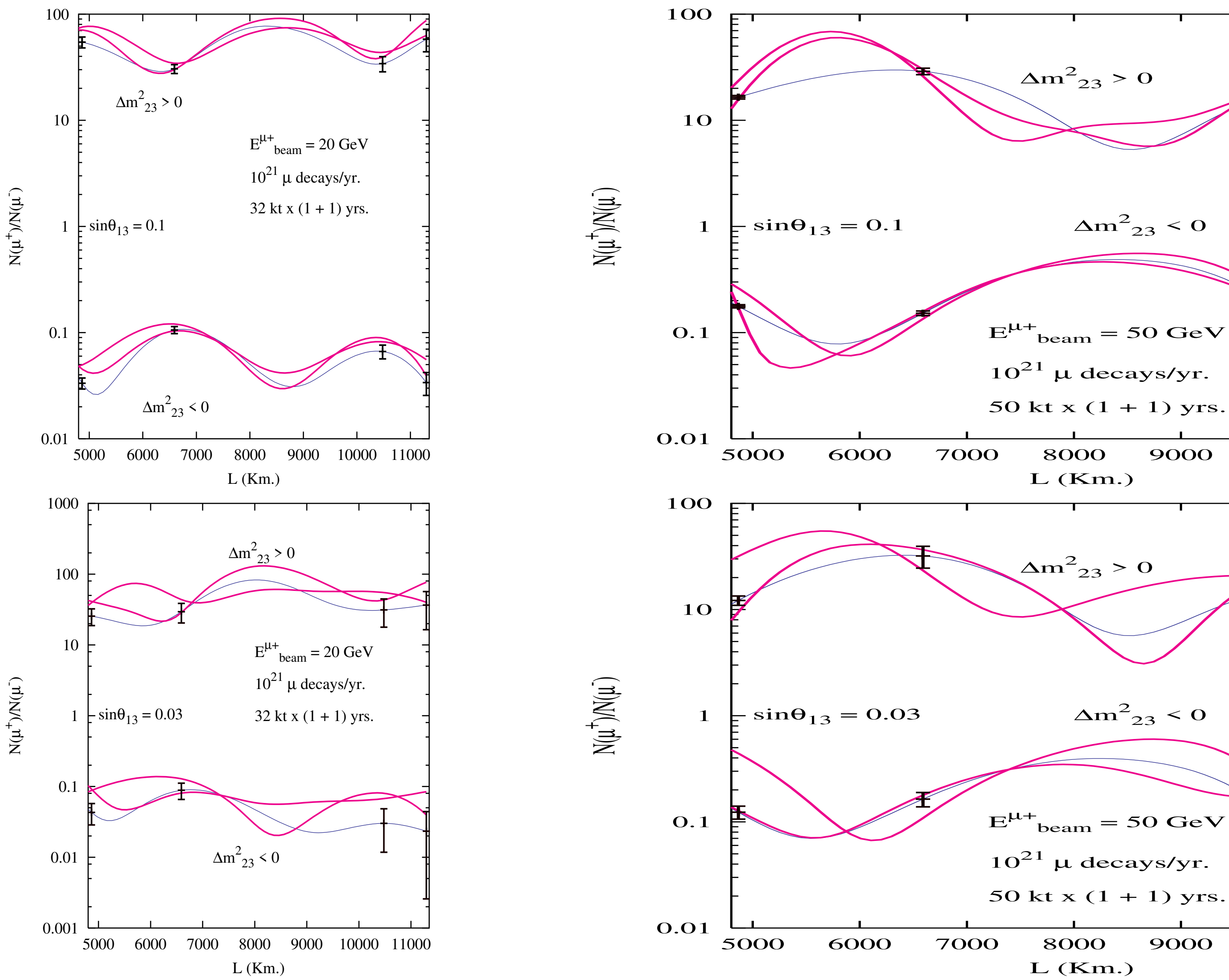

Figure 3.14: The same as Fig. 3.13, but for baselines corresponding to Fermilab–PUSHEP and Fermilab–Rammam along with the same ratios for JHF to the two proposed Indian sites. All other parameters are indicated in the plots. The data points with the sharp line through them are for $\delta = 0$. The other lines are for $\delta = \pm\pi/2$.

(6 in total) had unusual features which could not be explained away by any known processes of muons or neutrinos. They are characterised by the following features :

- The event consisted of two or more tracks, with at least one of them a muon or a pion as seen from their penetrating power without showering.
- All the tracks of the event seemed to originate from a vertex located either in air or thin detector materials - based on an extrapolation of projected angles of tracks.
- The tracks had a large opening angle ($\sim 45°$) between them, and
- Their rate was depth-independent and was a good fraction of neutrino events.

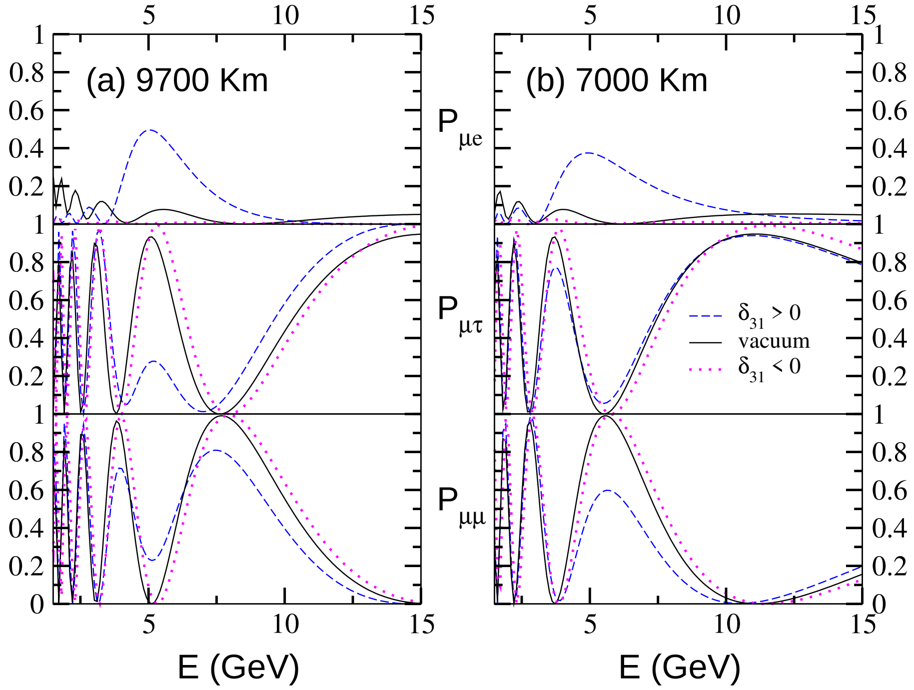

Figure 3.15: $P_{\mu e}$,$P_{\mu\tau}$ and $P_{\mu\mu}$ plotted versus neutrino energy E (in GeV) in matter and in vacuum for both signs of δ_{31} for two different baseline lengths, $L = 9700$ km and 7000 km. These plots use $\delta_{31} = 0.002$ eV^2 and $\sin^2 2\theta_{13} = 0.1$.

A number of theoretical attempts were made to understand the production processes [35] and see if they could fit into the prevailing schemes of particles and their interactions. The Kolar events have so far remained an enigmatic puzzle and they need to be studied with specially designed detectors that can address their special characteristics, such as ICAL.

Ultra high energy neutrinos and muons : The solar neutrinos have confirmed the basic hypothesis of stellar energy generation, while a handful of neutrinos from the supernova SN1987A have given insight into the mechanism responsible for supernova explosions. In a similar manner it may be possible to study of the interiors of other astronomical objects such as the Active Galactic Nuclei (AGN) through a study of high energy neutrinos from these objects. The phenomenon of Gamma Ray Bursts (GRB) suggests the possibility of the existences of such sources. Neutrino astronomy opens up a new window to the Universe and is thus an exciting new field with plenty of scope for surprises.

Detectors such as ICAL can also be utilised to study multi-TeV cosmic ray muons through their bremsstrahlung energy loss via the so-called pair-meter technique. Such studies in the TeV–PeV regions can throw light on possible extensions of the Standard Model in the high energy region. Calculations are in progress to determine the number of events at ICAL due to these ultra high energy (UHE) neutrinos and their signatures.

The motivation here is to study the knee in the cosmic ray primary spectrum. Cosmic rays are observed in a wide range of energies. The differential cosmic ray (CR) spectrum is a function of energy with a power law with index -2.7 up to an energy of $\simeq 4-7\times 10^{15}$ eV. This point is called the *knee* in the energy spectrum of CR. Beyond the knee it exhibits a different power law with index -3.1 up to an energy of $\simeq 5\times 10^{18}$ eV. This change in the behaviour of the CR spectrum at the knee poses a puzzle which can be resolved in two ways.

One way is to consider a different composition in the CR spectrum at the knee energy or above. A second way is to look for the missing energy taken by undetected particles produced at the knee. The known particles responsible for carrying the missing energy are neutrinos and muons. Existing detectors do not measure the energy of these particles and only count their numbers in CR showers. However with detectors like ICAL one would be able to measure the energies of these muons using the pair-meter technique. Using this technique one can estimate the event rate of muons for a few years running time, the number of interactions, energy of these high energy muons, etc. Calculations of this are underway.

Chapter 4

Numerical Simulations on ICAL

The primary focus of ICAL at INO is physics with atmospheric *muon neutrinos*. This implies construction of a detector that is sensitive to the energy, direction and charge (sign) of muons that are produced by charged-current interactions of the detector material with such neutrinos. This automatically implies that such a detector (perhaps upgraded in terms of fiducial volume) will also be a suitable choice as a far-end detector of a long-base-line experiment.

The detector geometry : The currently proposed detector is an iron calorimeter with magnetic field (ICAL). The detector design consists of 140 layers of 6 cm thick iron plates, with transverse dimensions of 32×14 m, separated by a 2.5 cm air gap containing RPCs or glass spark chambers which are the active detector elements. (The results discussed in the earlier chapters were for a width of 16 rather than 14 m; simulations corresponding to this revised size are in progress). The iron is assumed magnetised to 1 T; effects of non-uniform magnetic field are being studied.

The principle issues to be studied are charge identification and tracking (direction) and energy resolution for muons. The energy of hadrons can be reconstructed as well, but rather coarsely.

The neutrino source : The first stage involves a study of atmospheric neutrinos with the ICAL detector. The HONDA flux of atmospheric neutrinos has been used in the simulations. The main interactions in the detector are quasi-elastic (QE) and resonance (RS) interactions at low energies (upto a few GeV) and deep-inelastic scattering (DIS) at higher energies. Since the DIS cross-section is roughly proportional to the energy E, the events sample peaks around a few GeV although the flux itself peaks below 1 GeV. For "rock interactions" whose primary vertices are in the rock surrounding the detector, the events are at a much higher average energy.

4.1 Events generation

The NUANCE neutrino event generator [40] generates atmospheric neutrino events inside ICAL. A simplified ICAL detector geometry (with both horizontal and vertically oriented iron plates) has been encoded in the NUANCE generator. Basic cuts on the neutrino energies, $E > 0.8$ GeV, have been implemented while generating events themselves.

Events are generated using the HONDA flux [25] with some input oscillation parameters δ_{23}, θ_{23}, and θ_{13}. The last determines matter dependent effects which can be measured from charge-identification; we will only show results with $\theta_{13} = 0$. For neutrino energies greater than 0.8 GeV, neutrino charged-current (CC) events of interest are roughly generated in equal proportions via quasi-elastic, resonant and DIS processes. All results are shown for 5 years of accumulated CC events. Resolutions have also been obtained for 25 year sample for determining dependence on fluctuations. Typically interesting events have $E > 1$–2 GeV so the proportion of DIS events in the final sample is somewhat higher than the others. For this sample, the muon energy and direction are quite well correlated with that of the parent neutrino.

In summary, the energy of the interacting neutrino can be reconstructed by summing the energies of the muons and hadrons. Its direction can be deduced from that of the muon, while its particle type (particle or anti-particle) can be determined from the charge of the muon in the CC interaction.

A major issue, yet to be studied, is the mis-identification of pions as muons from NC as well as a subset of CC events and electron CC events.

4.2 The detector simulations package

A program based on the CERN library GEANT package simulates the detector response for the neutrino event, that is, propagates the muons and hadrons through the detector volume. The Fortran Version 3.2.1 is in use. A magnetic field map is in place although most of the results shown here are for a uniform magnetic field. Optimisation of the magnetic field with respect to both cost and physics issues is yet to be completed.

The digitisation of hits is done by assuming X and Y strips on the top and bottom of the RPCs of 2 cm width. Hence the spatial resolution of the detector in the x and y directions is assumed to be 2 cm. The layer number (in the z direction in the case of horizontally placed iron-plates, which is the standard configuration), gives the resolution in the z direction of 8.5 cm. The signal read-out can also contain module and tray information, which can be suitably transformed to the corresponding (x, y) values.

Dead regions due to housing of the magnet coils have not been simulated as yet. However, it is assumed that veto-counters on the top of the detector will veto the cosmic ray muons from above and help reduce this major background. This improves the fiducial volume.

The RPCs are assumed to give nano-second timing (for up/down discrimination). While it may not be possible to have sufficiently good time-resolution between successive hits, the requirement of minimum number of hits for reconstruction ensures that over-all timing efficiency and hence up/down discrimination is 100%. There is no energy information in a hit; all calibration is done by calibrating the track length (for muons) and number of hits (for hadrons).

4.3 Event reconstruction

Packages for event reconstruction—both of charge, energy and direction of muons and energy of hadrons in order to recover neutrino energy and direction. Independent packages (in C++ and Fortran) have been developed by two sub-groups in order to afford a cross-check on calculational results. Physics performance, that is, analysis of reconstructed events to extract physics. Here again two independent packages are available.

4.3.1 Muon energy reconstruction

In the absence of a magnetic field, the energy and direction of muons are reconstructed from the track length in the detector. A general formula for fitting a straight line in 3 dimensions is used to fit the track; the track length is then calibrated for known muon energies. It is found that the track length is proportional to the muon energy for almost all energies whose tracks can be contained. The charge of the muon cannot be identified in this case.

In the presence of the magnetic field, in addition, the muon momentum can be obtained from the track curvature and its charge from the direction of bending with respect to the external magnetic field. Partially contained events whose vertices are within the fiducial volume but whose track is not completely contained within can also be analysed in the presence of a magnetic field.

Consider a magnetic field applied in the z direction. The track bends in the x-y plane. Hence, there is a simple energy loss formula that determines the length of the track in the z direction, while a combination of energy loss and curvature in the external magnetic field determine the nature of the track in the x-y plane. The "transverse" momentum p_T is found by fitting to such a track in the x-y plane by determining the radius of curvature R_0 at the point of production. For a constant magnetic field, we have

$$p_T = \frac{3R_0(\text{ m})}{10B(\text{ Tesla})} \ .$$

The total momentum of the track is determined from $p_{\text{tot}} = \sqrt{p_z^2 + p_T^2}$. Several different methods of track fitting in the magnetic field have been tried. In some methods, the entire track length is used for fitting; such a procedure allows fits to totally contained events alone. In some methods, only about 30% of the length of the full track is used; this is useful to analyse partially contained events. The energy of muons with fully contained tracks can also be determined by summing individual lengths of track in the iron, as in the case where there is no magnetic field, since the magnetic field does no work. This serves as a cross-check on the calculations.

In Fig. 4.1 the distribution of the transverse momentum of the muon is shown using large number of muon triggers with constant $p_x = p_y = p_z =$ 3, 5, 7, 10 GeV or $p_T = 4.24(4.38 \pm 0.22), 7.07(7.01 \pm 1.47), 9.90(10.01 \pm 2.12)$, and $14.14(14.67 \pm 1.60)$ respectively, where the numbers in brackets are those determined from the fits to the tracks. The corresponding fits to the total momentum is shown in Fig. 4.2. A sample fit to the trajectory for fixed muon momenta of $p_x = p_y = 2, 5, 7, 10$ GeV using another technique is shown in Fig. 4.3.

4.3.2 Muon direction reconstruction

In the absence of the magnetic field, the direction of the muon is simply given by the slope of the straight-line fits to the tracks. In the presence of the magnetic field, since the muon is produced *in* the magnetic field, the "starting" direction of the track is a combination of the original muon direction and the effect of the field. However, some straightforward algebra helps determine the original muon direction (and hence the path-length L), provided the energy-loss in the medium is known. The figures Fig. 4.4 and 4.5 show the resolution obtained

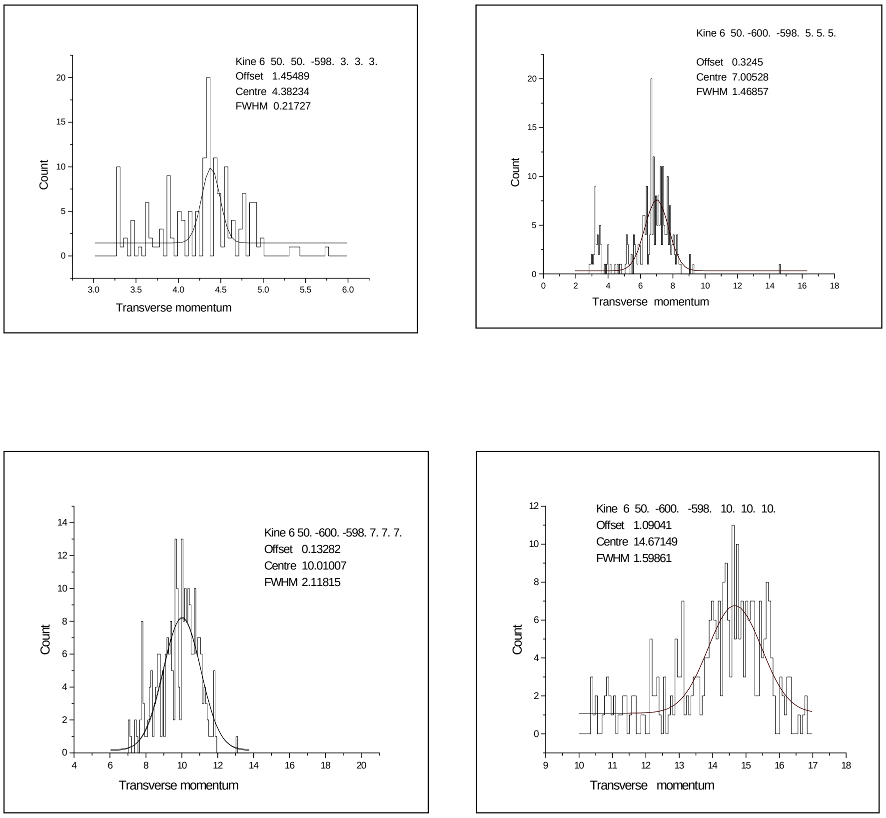

Figure 4.1: Distribution of the transverse momentum (p_T) of muon of incident momenta as discussed in the text.

in L (obtained from the zenith angle θ_z through $L = \sqrt{(R+L_0)^2 - R^2 \sin^2\theta_z} - R\cos\theta_z$) for 25 years of data simulation. The reason for generating a large data sample is to look for dependence of the resolution function on the mixing parameters that may bias the analysis; it is found to be independent of mixing.

4.3.3 Muon charge identification

Charge identification is crucial for matter effects when doing a three-flavour analysis. The charge of a particle is determined from the direction of the track curvature in the presence of

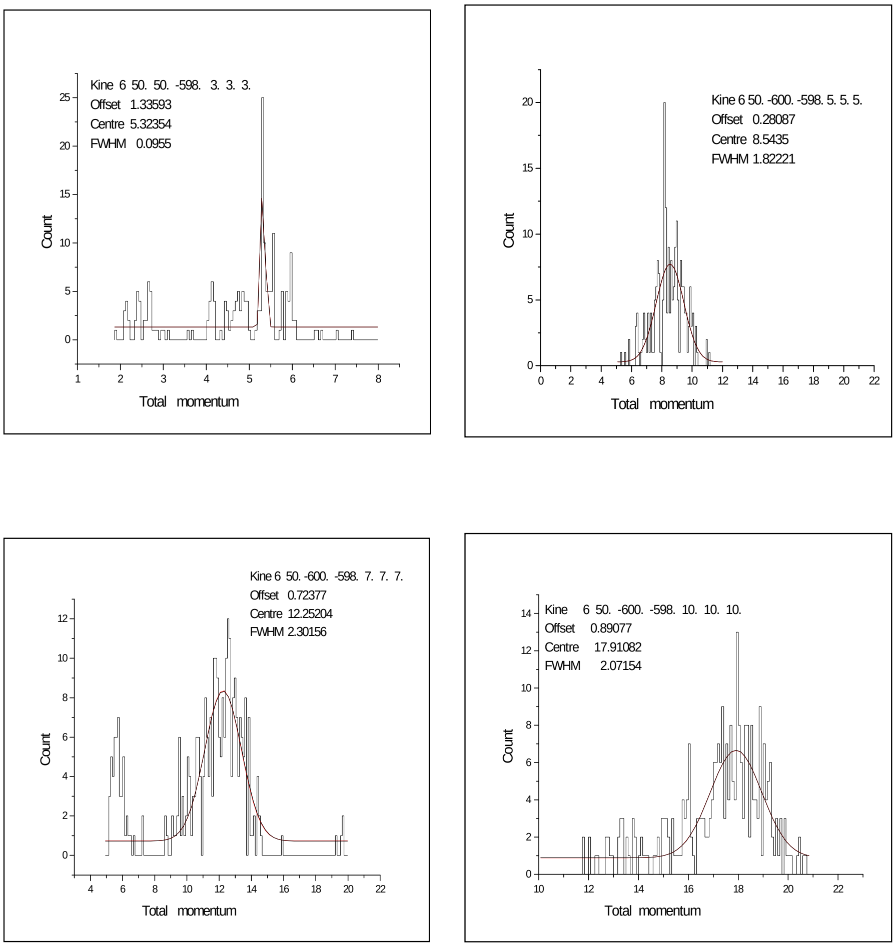

Figure 4.2: Distribution of the total momentum (p) of the muon corresponding to the same muon triggers as shown in Fig. 4.1.

a magnetic field. Different segments of the track as well as the entire track have been used for this purpose. Various methods all give roughly about 95% charge identification efficiency. For muon energies beyond 40–50 GeV, the track curvature is not sufficient to determine its charge. However, the set of such energetic muons from atmospheric neutrinos is small.

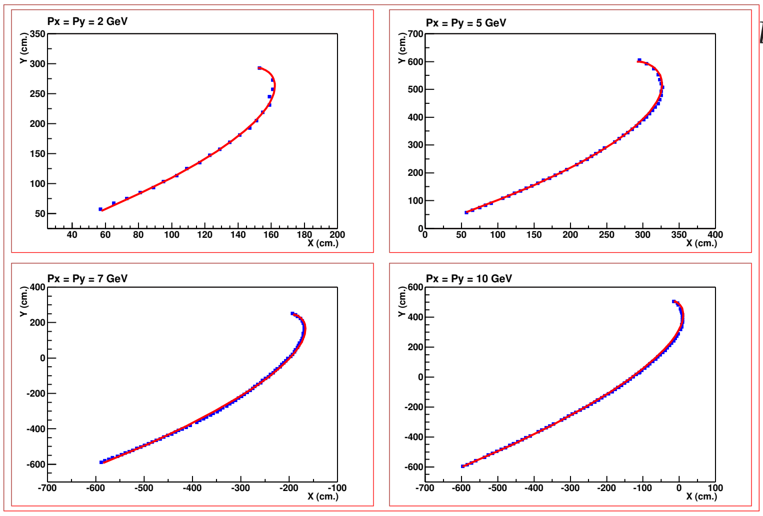

Figure 4.3: Sample fits to transverse tracks with momenta $p_x = p_y = 2, 5, 7, 10$ GeV respectively
.

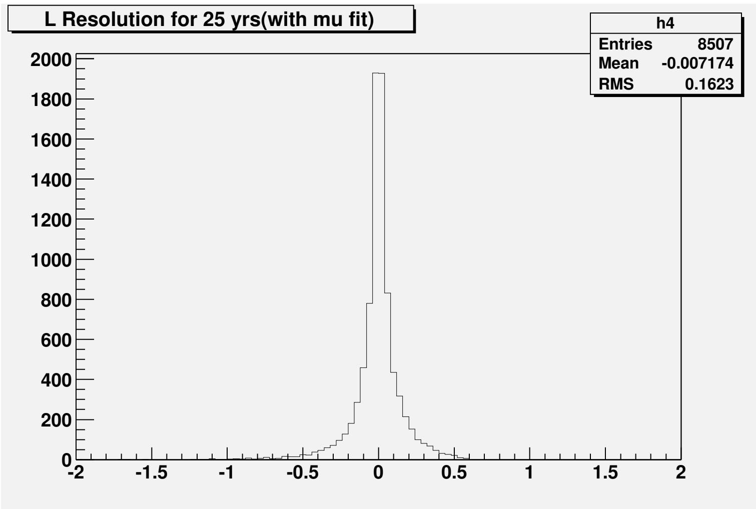

Figure 4.4: Zenith angle (L) resolution of muons is shown as the distribution of events as a function of $(L - L^{\rm reconstructed})/L$ where L is related to the original muon direction.

4.3.4 Hadron energy calibration

Since the atmospheric neutrino CC events of interest have substantial multi-pion events, the hadrons are calibrated using hit multiplicity. That is, the total hits (that are rejected as being part of the muon track) are calibrated to the total energy of the hadrons in the event. There is also no directional information in this approach. Hence, while calibrating, care has been taken to average the simulated tracks over all possible directions.

Fig. 4.6 shows the number of hits obtained from a sample of (25 years) atmospheric neutrinos, along with the calibrated best-fit to the data.

The resulting hadron resolution is shown in Fig. 4.7 where the resolution

$$\frac{\sigma}{E} = \frac{a}{\sqrt{E}} + b$$

is shown as a function of the total hadron energy E. The best-fit corresponds to $a = 0.31 \pm 0.063$ and $b = 0.30 \pm 0.003$ and is also shown in the figure.

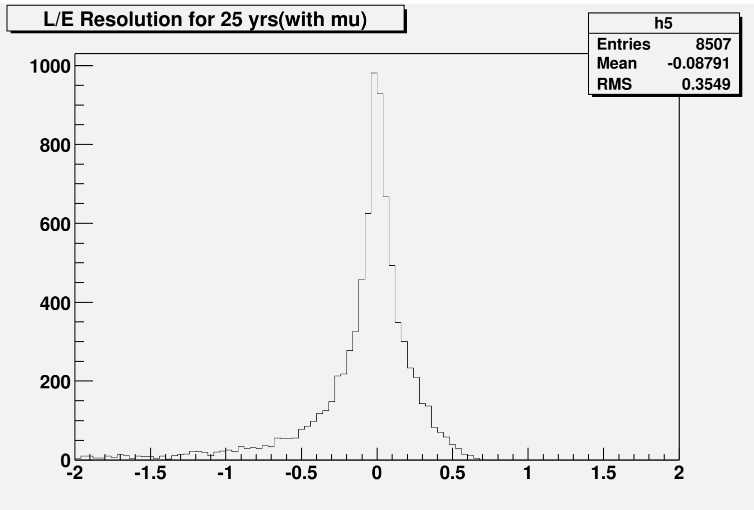

Figure 4.5: Zenith angle (L) resolution of muons is shown as the distribution of events as a function of $(L_\nu - L^{\mathrm{reconstructed}})/L_\nu$ where L_ν is related to the original neutrino direction.

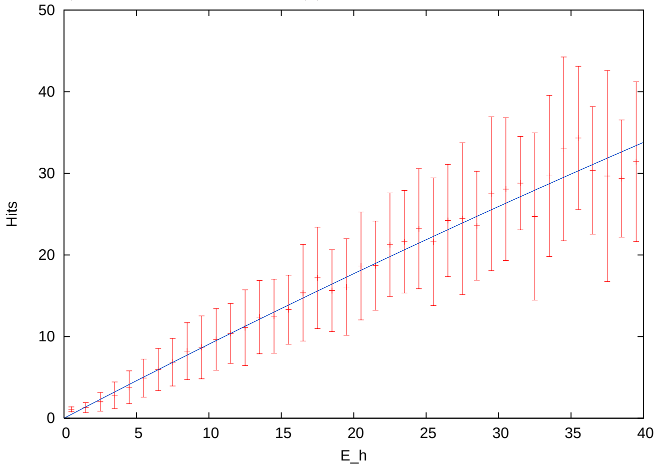

Figure 4.6: The number of hits as a function of the binned total hadron energy from a sample of 25 years of atmospheric neutrino events. The errors are not very sensitive to statistics and are dominated by the systematics of the hadron interactions in iron.

4.4 Study of atmospheric neutrino events

4.4.1 Analysis with horizontal detector plates

We use the NUANCE neutrino generator to generate atmospheric neutrino events with the HONDA flux. Two- and three-flavour oscillations are turned on within NUANCE although results presented in this section are for two-flavour oscillations alone. Sample sets of 5 and 25 years data are accumulated. The energy, E, zenith angle θ_z (and path-length L) and hence the L/E resolutions are shown in Fig. 4.8 for the 5-year data for both the fully contained (FC) and partially contained (PC) events. Both samples require the vertex to lie within the fiducial volume, with a cut on the zenith angle to remove very horizontal events ($\cos\theta_z > 0.156$). Furthermore, at least 7 hits in the muon track were required for the event to be included in the analysis sample. The combination of cuts already reduces the sample size to 40%.

In the absence of a magnetic field, resolution functions can also be calculated for the restricted sample of only FC events using the calibration of the energy in terms of track-length.

Using these resolution functions, the input data are analysed for the ratio of up/down

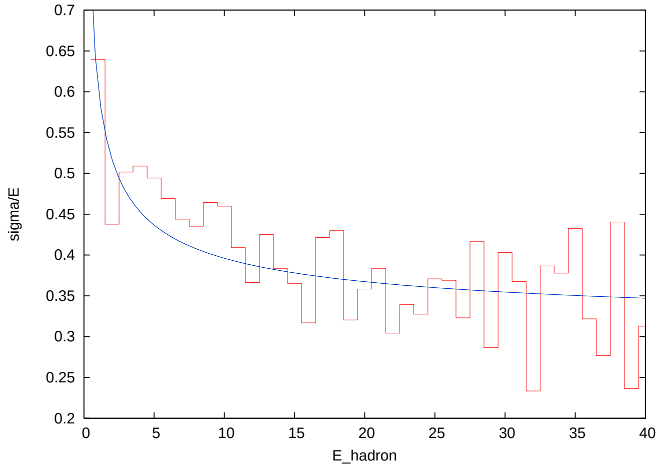

Figure 4.7: Calibration of hadron energy resolution from a sample of 25 years of atmospheric neutrino events.

events, as explained in the Physics chapter. The average 2-flavour survival probability is given by

$$P_{\mu\mu}(L/E) = 1 - \sin^2 2\theta_{23} \sin^2 \frac{1.267\delta_{32} L}{E} \ .$$

Data were generated by NUANCE for $\sin 2\theta_{23} = 1$ and $\delta_{32} = 0.5, 2, 3, 7 \times 10^{-3}$ eV^2. The tracks were obtained by passing the sample through the GEANT package and the L and E recovered. Note that the analysis uses the mirrored L (with $\theta \to \pi - \theta$) for the down-going neutrino events. The up/down events ratio is plotted in bins of $\log_{10} L/E$ in Figs. 4.9 and 4.10. A comparison with the theoretical $P_{\mu\mu}$ is possible only when the latter is smeared with the detector resolution in L/E:

$$P_{\mu\mu}(x) = \int \mathrm{d}x' R(x, x') \left(1 - \sin^2 2\theta_{23} \sin^2 1.267\delta_{32} x'\right) \ ,$$

where the resolution function is given by the Lorentzian,

$$R(x = L/E) = \frac{1}{\pi} \left(\frac{\sigma/2}{(\sigma/2)^2 + (x - x')^2}\right) \ ;$$

σ is the width in L/E of the ICAL detector. (When a three-flavour formula is used, the survival probability is independently a function of L and E; in this case, individual resolutions in L and E, with a corresponding two-dimensional integration over the true E and L values must be used.)

The resolution obtained, in the absence of magnetic field, for muons only, is

$$\sigma = 0.18 \, \frac{L}{E} \ .$$

This was applied to a sample of events generated using the mixing parameters,

$$\delta_{23} = 3 \times 10^{-3} eV^2; \sin^2 2\theta_{23} = 1.0 \ .$$

The sample was binned for its up/down events ratio as a function of L/E and fitted to the theoretical expression in Eq. 1 to obtain a best fit to the oscillation parameters of

$$\delta_{23} = (3.3^{+0.3}_{-0.6}) \times 10^{-3} \text{ eV}^2; \quad \sin^2 2\theta_{23} = 0.98^{+0.02}_{-0.07} \ .$$

The binned data and the fit to it is shown in Fig. 4.11.

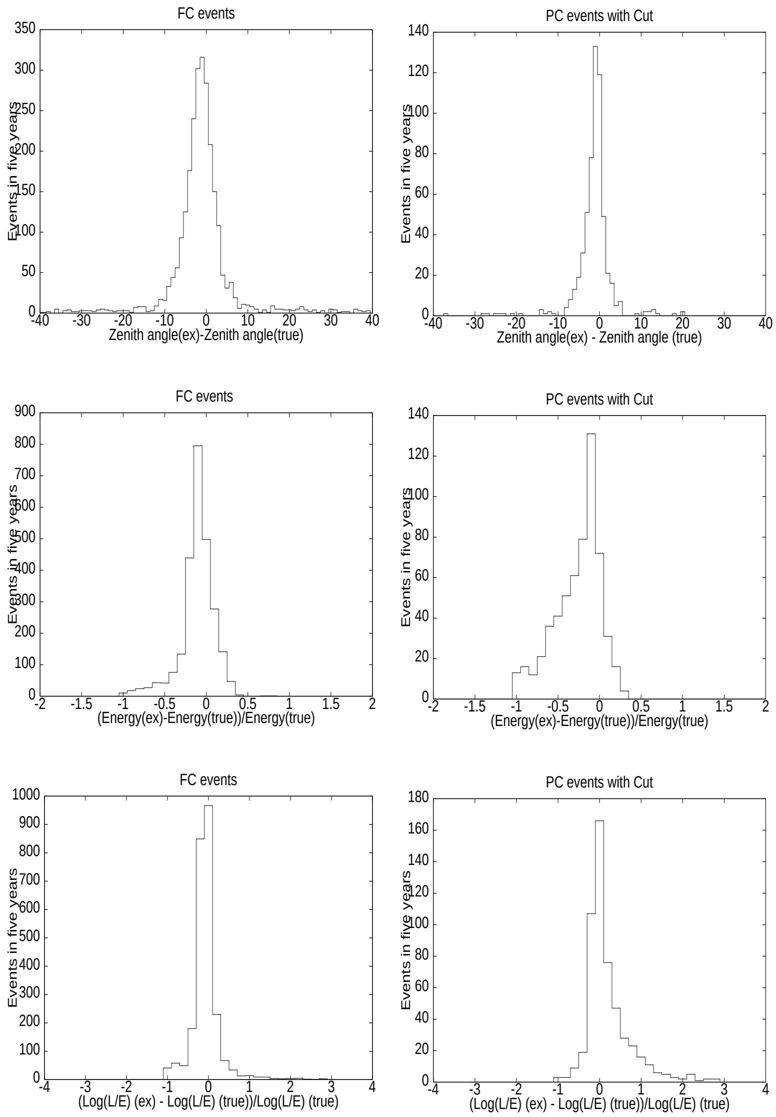

Figure 4.8: Top: ICAL zenith angle resolution for fully-contained (left) and partially-contained (right) 5-years events sample after the selection cuts. Centre: Neutrino energy resolution. Bottom: L/E resolution. The selection cuts are discussed in the text.

4.4.2 Analysis with vertical detector plates

As can be seen from the analysis so far, the best sensitivity to mixing parameters is when the first dip (or oscillation maximum) is in the range of $\log_{10} L/E \sim 2$–3. There are few events at smaller L/E; this is a combination of an upper limit on energy reconstruction and a lower limit on the path-length L. The latter occurs because the horizontal plates restrict the maximum detectable zenith angle to 84° ($\cos\theta > 0.156$). Below this value, there are very few events that satisfy the analysis criterion of at least 7 hits in a muon track, due to the horizontal nature of such events and the detector geometry. It was therefore natural to ask whether a detector geometry with *vertical* iron plates would be more sensitive to the up/down ratio. Since the plates are in the vertical configuration, there is now theoretically no lower limit to $\cos\theta_z$ and it is possible to enhance the statistics in these low L/E bins.

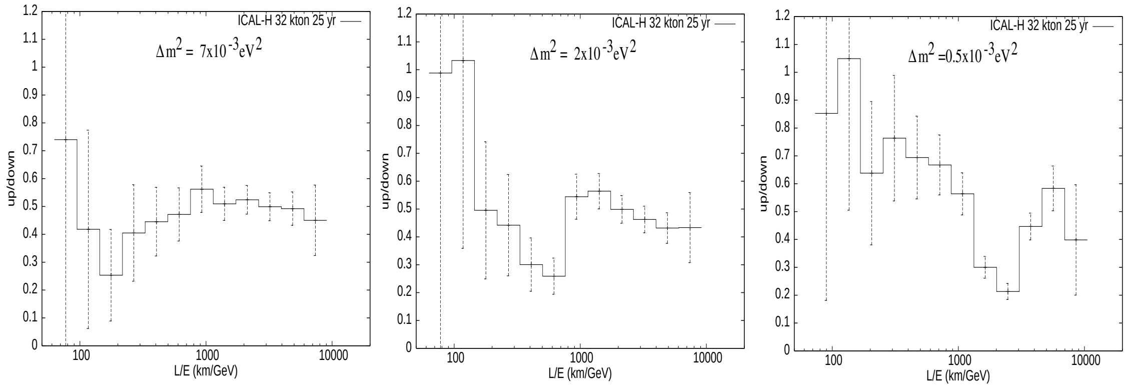

Figure 4.9: The ratio (up/down) as a function of (L/E) for ICAL for the choices $\Delta m^2 = 7 \times 10^{-3}, 2 \times 10^{-3}, 0.5 \times 10^{-3}$ eV^2 respectively and $\sin^2(2\theta)$=1.

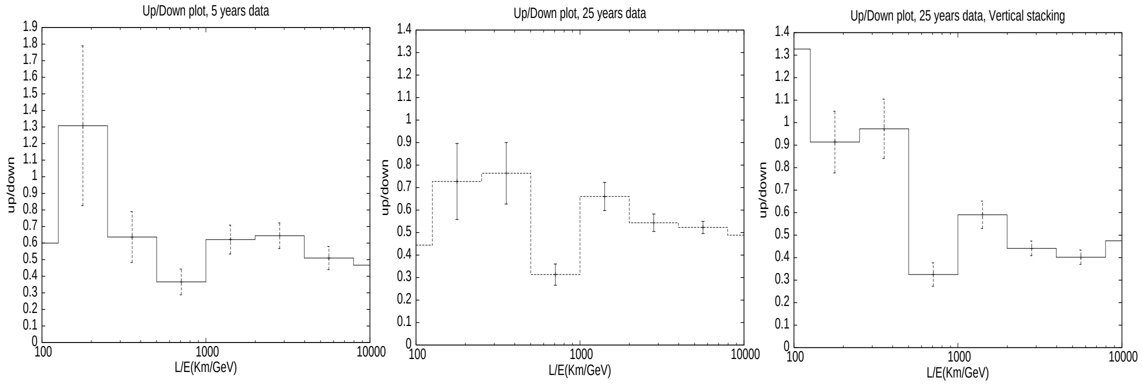

Figure 4.10: The ratio (up/down) as a function of (L/E) obtained from PC+FC events in 5-year ICAL-H (left), 25-year ICAL-H (center) and 25-year ICAL-V (right). For these plots $\Delta m^2 = 2 \times 10^{-3}$ eV^2 and $\sin^2(2\theta)$=1.

Such a configuration may also have a bearing on the possibility of using such a detector as a far-end detector in a long-baseline experiment.

The results of such a vertical geometry are shown in the subsequent figures. The geometry uses iron plates stacked vertically in the x-direction with x-y-z dimensions 12 m $\times$ 32 m $\times$ 14 m.

Cuts on energy and zenith angle of $E > 1.5$ GeV and $|\cos\theta_z| \leq 0.988$ are used to cut out vertical events ($\theta_z > \pm 9^\circ$); the latter to satisfy criteria on minimum number of hits in the track. Furthermore, a cut of $|\cos\theta_z| \geq 0.052$ ($\theta_z < \pm 87^\circ$) is used to cut out horizontal events (for up/down discrimination). The figure Fig. 4.12 shows that smearing of the up/down events causes the dip in the up/down events ratio to virtually disappear. This clearly indicates that, though the muons are generally in the direction of the original neutrino, at very large zenith angles, even a small mis-match between the two can cause an "up" event to be identified as a "down" event and vice-versa. In fact, as can be seen from Fig. 4.13, when the cut on the zenith angle is put back at $\cos\theta_z > 0.156$ (as with the horizontal geometry analysed so far), the dip in the up/down ratio re-appears; however, there is then no improvement in the statistics of the low L/E bins. In fact, the fit especially

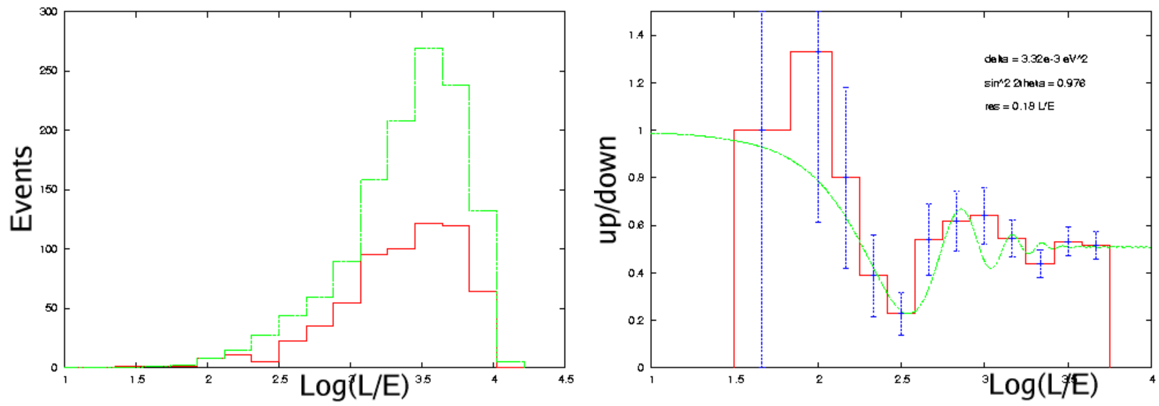

Figure 4.11: Left: up, down events as a function of L/E. Right: up/down ratio as a function of L/E along with a best-fit curve with parameters as shown/given in text.

to $\sin\theta_{23}$ becomes very poor in the case of vertical ICAL, as can be seen from Fig. 4.14.

Hence, the merits of ICAL with a vertical geometry have to be carefully analysed, keeping in mind the tension between the requirement for improvement of statistics and fidelity in recovery of neutrino oscillation parameters.

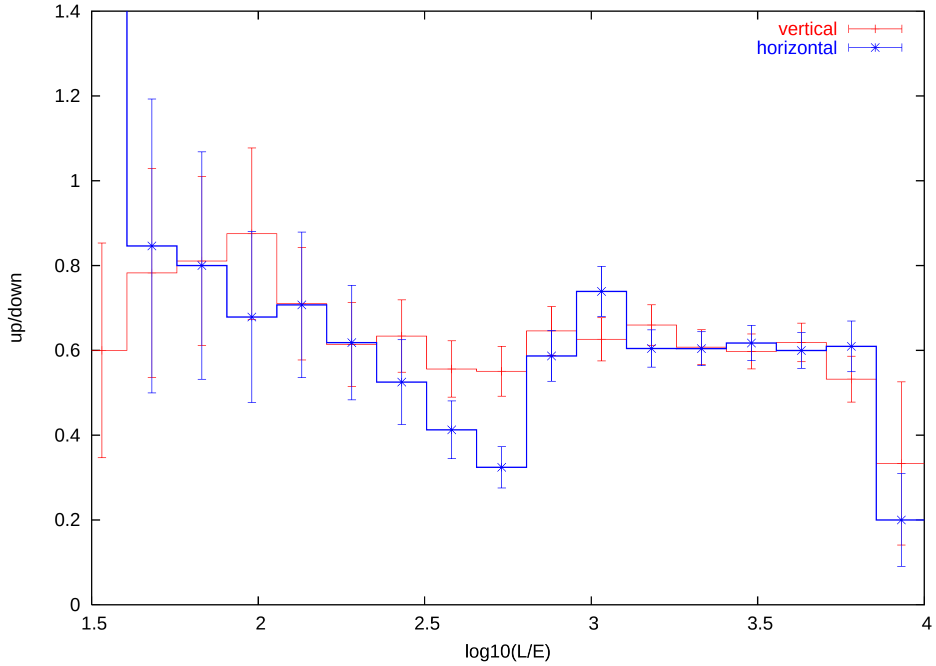

Figure 4.12: Up/down events ratio with a zenith angle cut of $\cos\theta_z > 0.052$ as a function of $\log_{10} L/E$ for $\theta_{23} = 45°$ and $\delta_{32} = 2 \times 10^{-3}$ eV^2 for a vertical ICAL geometry. The results with a horizontal geometry are shown as darker (blue) lines in comparison; the latter analysis uses $\cos\theta_z > 0.156$.

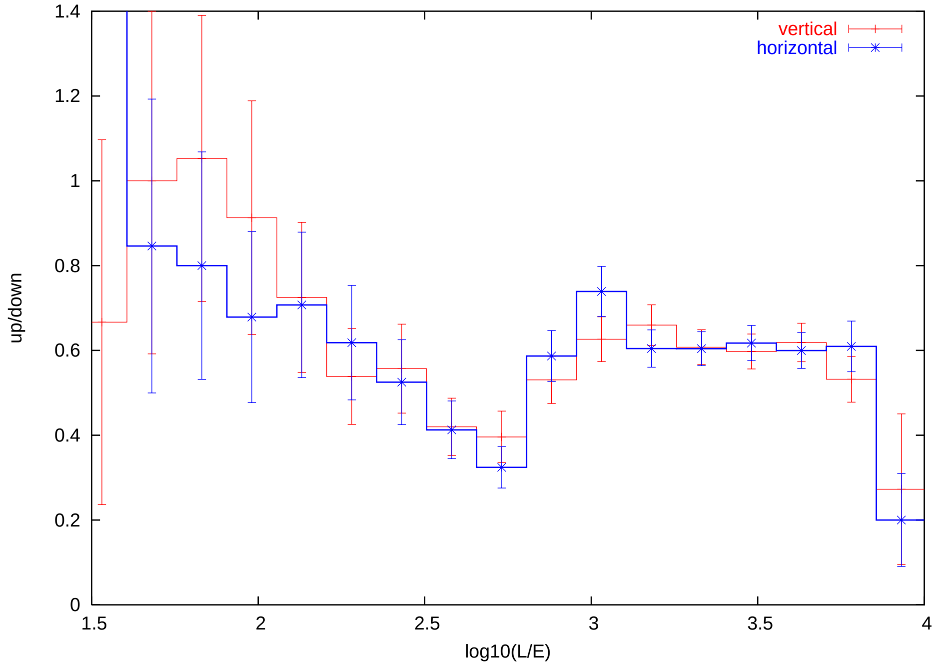

Figure 4.13: Up/down events ratio with a zenith angle cut of $\cos\theta_z > 0.156$ as a function of $\log_{10} L/E$ for $\theta_{23} = 45°$ and $\delta_{32} = 2 \times 10^{-3}$ eV^2. The results with a horizontal geometry are shown as darker (blue) lines in comparison; both samples are analysed with the same zenith angle cut.

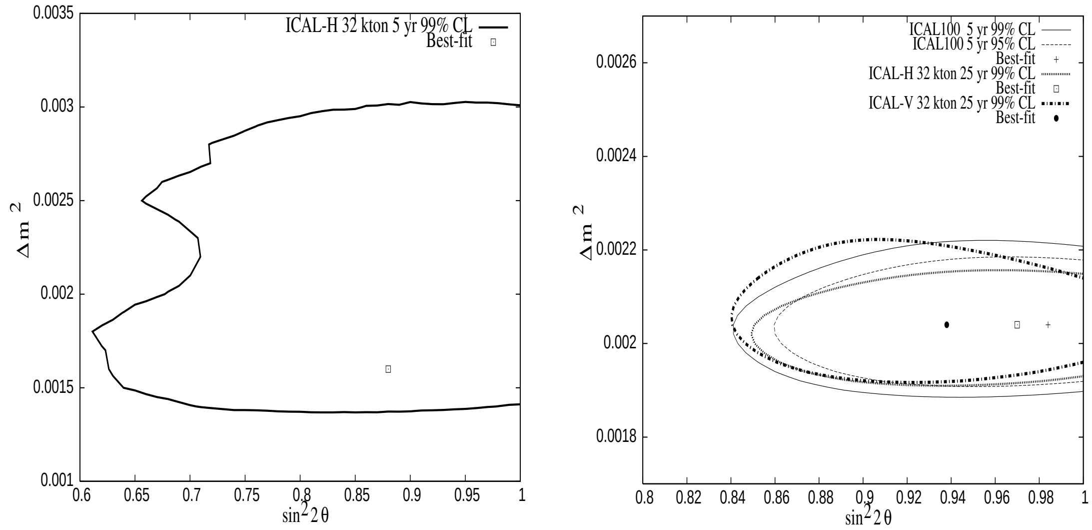

Figure 4.14: The 99% C.L. allowed regions and the best-fit values in the $\Delta m^2 - \sin^2(2\theta)$ parameter space for 5-year ICAL-H run (left panel) and 25-year ICAL-H, 25-year ICAL-V, and 5-year ICAL100 runs (right panel) obtained using fully-contained events and no magnetic field. The input data had neutrino oscillations with $\Delta m^2 = 2 \times 10^{-3}$ eV^2 and $\sin^2(2\theta)$=1.

Chapter 5

Tale of two (three) sites

An important component of the INO feasibility study is to find an appropriate location with sufficient rock overburden to satisfy the physics objectives. This section outlines the results of the various surveys undertaken in many places all over the country. This has been necessitated by the fact that one of the best sites available in the world, namely KGF, is not accessible for experiments any more. We first outline the set of criteria which were used to determine the suitability of the sites surveyed for the location of INO.

The site survey group studied the topographic material and discussed with scientists of the Geological Survey of India and the engineers involved in many underground projects regarding many possible sites in the Western Ghats of South India, the lower Himalayan region in West Bengal. Based on a set of criteria evolved for the purpose, two particular sites located near PUSHEP at Singara in the Nilgiris and Rammam in Darjeeling have been identified as the possible sites. A summary and comparison of these possible sites is given below. Of of these two sites will eventually be chosen to house INO. Apart from these, another exciting possibility appears to be the 8,800 meters long tunnel under Rohtang Pass near Manali.

5.1 Site Requirements

In order to have some uniform criteria to prepare a report on possible sites for INO, the following criteria were suggested[1]:

The recommended evaluation criteria may include the following factors :

1. History of the site: This mainly translates to the issue of availability of the site on a long-term basis.

2. Cost factors: This includes both construction costs and operating costs. Existing underground projects like hydro-electric plants are better since many of the facilities such as access roads and housing would already be present and save costs.

3. Risk Factors and Safety issues:

[1]These criteria were obtained from our own experience as well as by looking at similar studies in other locations, especially the documents related to the proposal for a National Underground Science Laboratory in the US [18]. We have benefitted much from these earlier or ongoing projects.

- Rock conditions risk: This risk factor includes multiple considerations relative to the risk of capital and operating cost overruns due to unexpected rock conditions. Forecasting based on known stress conditions may help in anticipating such a risk.
- Environmental Risk: The time and expense required at various sites to determine what is safe and environmentally sound.
- Seismic Risk: Although engineering can control seismic risk, there is an additional cost involved in installing detectors in a seismically active region. In addition, there is a risk of a more intense than expected earthquake or an engineering or installation mistake that leads to failure in an earthquake of expected magnitude.
- Mechanical Systems Risk: Sites with heavy equipment, hoisting or other machinery have an operating cost risk due to the possibility of failure of significant mechanical systems.

4. Depth: Apart from a reasonable overburden in all directions, a complete 3D topo map of the region must be prepared for evaluating backgrounds. Rock density, suitability for low radioactivity experiments, are other factors.

5. Neutrino Beam: Though this is still some way into the future, distances to various neutrino factories and any particular advantage that may be there due to physics reasons is an important factor.

6. Time to Install First Detectors: This is perhaps the most important factor for INO to be competitive.

7. Accessibility: Access to the laboratory by air/train/road throughout the year is an important factor. The perceived ease of personnel access to the laboratory is important both as a substantive factor and as a quality-of-life factor. Ideally, the laboratory should be available 24 hours a day, seven days a week.

5.2 Summary of the sites

Details of the location, geology and physics prospects at both PUSHEP and Rammam sites are available. The topography is well-known as well as the rock-type and quality. Some highlights of the two sites are presented below, followed by a comparative study of the two locations.

PUSHEP Site: This site located in Singara in South India (Lat. North 11.5° and Long. East 76.6°), situated in the southern peninsular shield, offers one of the best tunnelling medium for the creation of an underground facility. If located here, the INO site will be an extension of an almost-operational underground Hydel project located about 6.5 kms from a town called Masinagudi (90 km south of Mysore) at the edge of the Mudumalai sanctuary near the borders between Tamil Nadu, Karnataka and Kerala states. It is called the Pykara Ultimate Stage Hydro Electric Project (PUSHEP) and is being executed by the Tamil Nadu Electricity Board (TNEB). The powerhouse is located in a cavern 500 m underground, accessed by a 1.5 km long tunnel. Fig. 5.1 gives a panoramic view of the PUSHEP site.

Figure 5.1: A View of PUSHEP location from Glenmorgan.

Figure 5.2: Panoramic view of the Mountain at PUSHEP. The laboratory cavern will be located directly under the peak (2207 meters).

The underground cavern is 20 meters wide, 39 meters high and 70 meters long, so its dimensions are similar to the requirement of INO for locating the iron calorimeter detector. The prior existence of a number of tunnels is important for future forecasting. The site is also conveniently located in seismic zone-2, which implies a minimum seismic activity zone in India. A panoramic view of the peak directly above the projected site is shown in Fig. 5.2.

Rammam site: The INO site near the Rammam hydel project is located in the Eastern Himalayas (Lat. North 27°24′ Long. East 88°05.5′) in the district of Darjeeling in the state of West Bengal. It is at an elevation of 1450 m and is about 140 kms away from Bagdogra airport and the city of Siliguri. Bagdogra is connected by air to both Kolkata (1 hr flight time) and Delhi airports. Siliguri is connected by train to Kolkata (overnight journey) and to Delhi. It takes about 6 hours by car to reach Rammam from Bagdogra/Siliguri. There are three alternate routes. The scenic hill town of Darjeeling, the district headquarters is closer—about 70 kms (2.5 hrs) away—and again connected by two alternate routes.

The Rammam hydel project presently has an installed capacity of 4×12.75 MW. It uses the water from the Rammam river and in its future extension plans will utilise the water from the other river Lodhama as well.

The proposed portals of the INO access tunnel and adit are located adjacent to the metalled road leading to the powerhouse (about 4 km south) of the hydel project. They are within the hydel project settlement and connected through a network of metalled/non-metalled roads. Figs. 5.3 and 5.4 show photographs of the area at the proposed portal location and a panoramic view from there. Multiple locations and depths for the laboratory are possible. The area is in seismic zone 4.

Figure 5.3: INO tunnel portal location at Rammam Site.

Hence extra precautions need to be taken during the construction stage. A number of long tunnels and large caverns already built in and around this area stand testimony to the feasibility of tunnel construction in this area.

Rohtang Pass Site: Apart from INO at PUSHEP and Rammam, another exciting possibility is the 8,800 meters long tunnel near the Rohtang Pass at Manali. Two important reasons that make this site particularly exciting are that only a cavern/chamber needs to be excavated and that the overburden may be more than any other site that has been surveyed until now.

The Rohtang tunnel will bore through the Pir Panjal range in the Himalayas from Kullu-Manali valley into Lahaul-Spiti valley. The south portal is at an elevation of 3050 m and the north portal is at an elevation of 3080 m. The maximum vertical overburden is 1900 m about

Figure 5.4: Panoramic view of the Rammam river valley.

6 km from the south portal. Veering to the left from the south will achieve overburdens well in excess of 2000 m.

At the proposed Rohtang road tunnel, there will be ventilation ducts on both sides, fire hazard monitoring cells, traffic hazard cells and even pollution monitoring cells. The road tunnel will be 10 m wide, 10 m high in horse-shoe shape allowing two-lane traffic. The overburden exceeds 1000 m in a length from about 3.8 km to 6.8 km from the south portal. Access to the tunnel is from Manali or near about. There is a small airport at Kullu which is connected to Delhi by air. The nearest railhead on broad gauge is nearly 300 km away. However Manali is connected by road to Shimla, Chandigarh and New Delhi.

One major civil engineering task will be automatically achieved because the 8.8 km long tunnel provides multiple locations where caverns may be excavated as has been done at LNGS in Gran Sasso. It will have a much greater overburden than any other underground laboratory in the world, rivalled only by the underground facilities that existed at KGF. The photograph in Fig. 5.5 shows a panoramic view of the area. The Border Roads Organisation (BRO) is likely to create a campus around the beginning of the tunnel near Manali to provide dedicated power supply, ventilation system, water supply and fire services on such a large scale that the needs of the INO laboratory will be a marginal addition. This fact alone gives a tremendous advantage for INO since many of the maintainance aspects are already built-in. Furthermore, the construction of caverns and smaller tunnels may also be undertaken by the same organisations that are involved in the Rohtang tunnel project on a turnkey basis for INO.

While these factors make this proposal promising there are some issues, minor or major, that need further study:

- The project site is situated in Seismic Zone-4 after recent reclassification.

- The time scale of the proposed project is expected to be between seven to nine years from the start date which is 2005.

Figure 5.5: View of the Rohtang Pass from the highest point at 3980m. The winding approach road from Manali is visible.

- There are several avalanche points along the access road to the south portal which need to be continuously managed. Furthermore, the area near the portal will be snow bound with heavy snow in winter. While the agencies may clear snow to keep the tunnel operational, it is likely to create delays both during construction and operation.

5.3 Tunnel and Cavern Complex

The description given below provides a feasible baseline access and laboratory designs that satisfy the scientific needs of INO. These may change depending on detailed geological mapping of the site and as the INO needs are fully developed. No finality in design is presumed.

Surface laboratory and portal: Once the location of the portal is decided at a chosen site for INO, an important next step is the extent and availability of land for surface laboratories, if any.

Design of access tunnel: There are two feasible options for the design of tunnels: single tunnel or two tunnel access. The main factors that will dictate the appropriate option will be cost and safety issues. While the single tunnel option is cost effective, the twin-tunnel is expensive but safer.

Cavern complex: The orientation of the cavern complex is tentatively fixed as running from North to South in PUSHEP extrapolating from the geotechnical data available at present. The exact location and orientation of the underground complex depends on the detailed data that will be obtained and monitored as the tunnel construction progresses in

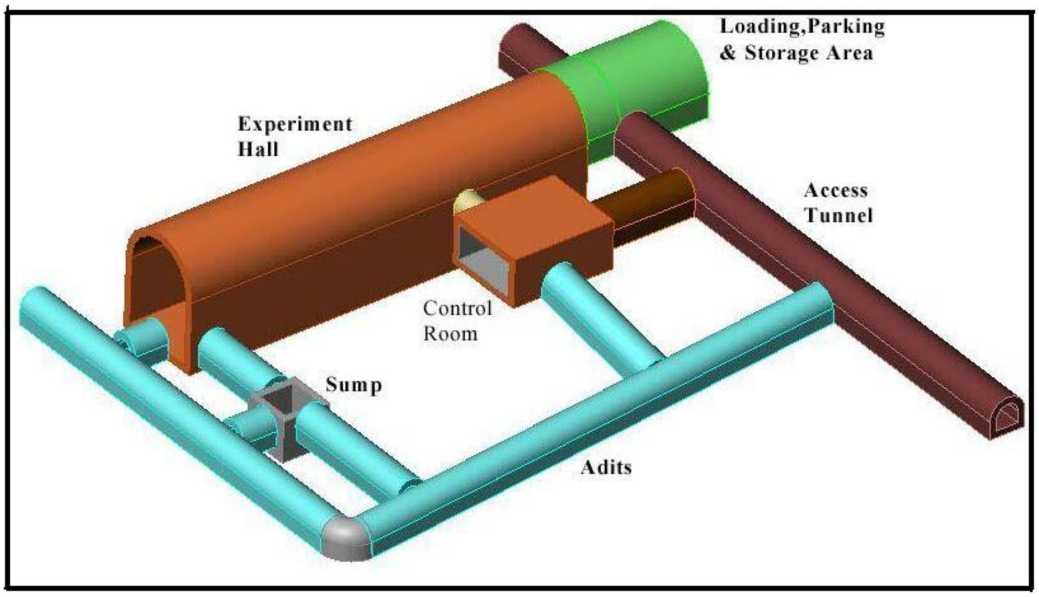

Figure 5.6: An artist illustration of the Laboratory Cavern Complex

the chosen site. A schematic view of the cavern complex based on the present design of PUSHEP powerhouse complex is given in Fig. 5.6.

5.4 Comparison of PUSHEP and Rammam

The atmospheric muon background flux at these two sites may be obtained from Fig. 5.7 where the depth is measured in metre-water-equivalent, MWE (depth times the density of matter). Corresponding depths of some well-known labs are indicated in the figure for comparison. Other features of INO at PUSHEP and Rammam are summarised in Tables 5.1 and 5.2.

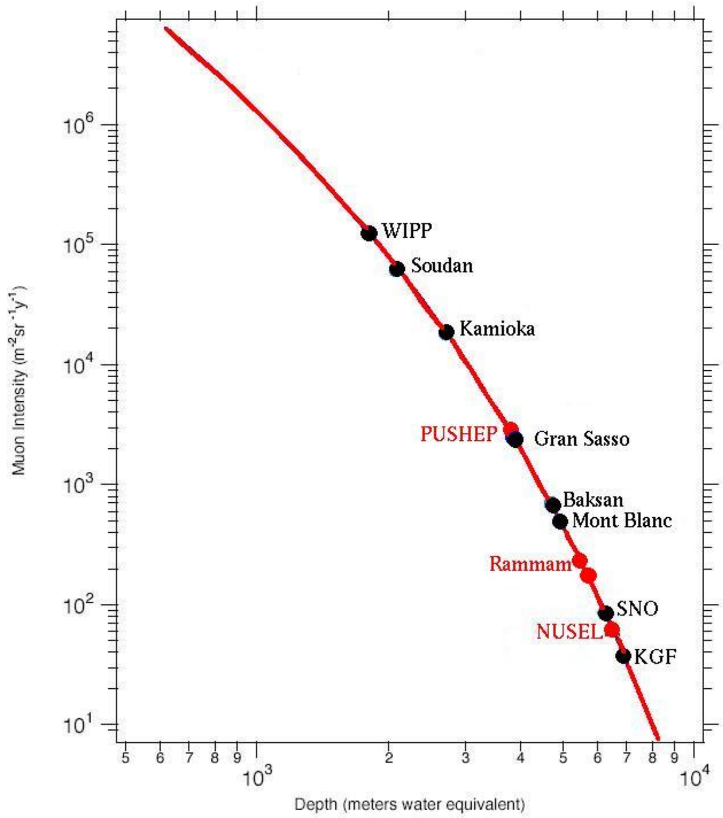

Figure 5.7: Atmospheric muon background as a function of depth. The best locations for INO correspond to backgrounds as in Gran Sasso or better. The Rohtang site is not shown, but the background may be comparable to KGF if not better.

Criteria	PUSHEP	Rammam
1. Site History:	Singara project since 1930s; PUSHEP built to last 100 yrs	Operating since 1995
2. Transportation: Site access:	 Masinagudi (7 km) Ooty (30 km) Mysore (90 kms) Coimbatore (100 kms) Calicut (120 kms) Bangalore (250 kms)	 Lodhama (5 km) Darjeeling (70 km) Siliguri (140 km)
Nearest Railhead:	Mysore (North) (90 km) Coimbatore (South) (100 km) Calicut (West) (120 km)	New Jalpaiguri (150 km)
Nearest Airports:	Coimbatore (domestic) Calicut (domestic) Bangalore (Int'l)	Bagdogra (domestic) Kolkata (Int'l)
3. Geotechnical Data: Rock type: Specific gravity: Q-factor of tunnel. medium: Horizontal/vertical stress ratio (1–2 is desirable): Seepage: Geological adversities: Geological mapping: Stand up time: Support measures: Rock radio-activity:	 Charnockite (Monolith) 2.62–2.9 4-45: Good to very good Approximately 1.6 Moist to Dry No known adversities Shears, dykes, joints are mapped from both surface projections and underground tunnels 90 days to infinity PCC lining, shotcreting, rock bolting 0.005 mR/hr—very low	 Gneiss 2.79–2.84 Fair to very good Not available Moist No known adversities Shears, joints are mapped from surface studies 1–90 days shotcreting, rock bolting Not available
4. Neutrino beam base-line: CERN (Magic baseline) JHF Fermi Lab CHECK THIS	 7,100 km 6,600 km 11,300 km (with 2,400 km of core)	 7,100 km 5,000 km 10,600 km (no core)

Table 5.1: Comparison of various features at PUSHEP and Rammam, to be continued in Table 5.2.

Criteria	PUSHEP	Rammam
5. Laboratory Features:		
Lab Location:	Below 2207 m at ≈ 900 m above MSL	Below 2880 m at ≈ 850 m above MSL
Lab Access:	Horizontal two way heavy equipment transport	Same
Tunnel Option:	Tunnel Length (km); Vertical Cover (m); All-round cover (m)	
Option-1	1.87; 1313; ≥ 1000	3.25; 1400; ≥ 1250
Option-2	2.13; 1299; ≥ 1000	3.85; 1680; ≥ 1500
Option-3	2.38; 1340; ≥ 1000	4.85; 1780; ≥ 1650
Gradient:	1:15 (reverse)	Horizontal
6. Risk Factors:		
Seismic Risk:	Zone-2 No discernible faults	Zone-4 No faults on alignment
Environmental Risk:	Reserve Forest Portals are inside TNEB/private land	Reserve Forest Portals are inside WBSEB/Govt. land
Civil Unrest/Terrorism:	None so far	None so far
7. Time Scale :		
Pre-Construction Stage:	≤12 months	≤ 12 months
Tunnel/cavern excavation with support measures:	About 22 months	About 41 months
Mechanical Outfitting:	12–18 months	12–18 months
8. Cost Saving Factors:		
Facilities already available:	Housing, guesthouse, access road, security guesthouse at Ooty	Housing, guesthouse, access road, security
9. Academic Institutions:		
Educational Inst.:	Bangalore, Mysore, Coimbatore, Calicut	Siliguri, Darjeeling
Research Inst.:	Bangalore, Mysore, Coimbatore, Ooty (TIFR RAC/CRL)	Darjeeling, Kolkata
10. Environmental Factors:		
Weather:	Moderate (min. 12–25°C)	Moderate (min. 5–20°C)
Rainfall/year:	Low (100–150 cm)	Mod. heavy(300–400 cm)
Access:	24 hrs/365 days	Almost all days
Biosphere:	Wildlife sanctuary	Wildlife sanctuary

Table 5.2: Comparison of various features at PUSHEP and Rammam, continued. The time factors for driving tunnels and cavern construction are based on L&T estimates and are to be regarded as approximate guide-lines.

Chapter 6

Strategies for Human Resource Development

INO will require a substantial investment in human resources. We have to train a large number of physicists and engineers who will ultimately be the backbone of INO and contribute to its success. Innovative ideas are needed in the recruitment and training of these physicists. Some of the INO members have already started giving lectures to students in colleges, universities and other institutions, exposing them to recent discoveries in neutrino physics and to the possibility of doing front-line neutrino experiments in India. While a lot of interest has been expressed by students on INO, we do not have a suitable mechanism, as yet, to exploit this abundant resource available in the country. This will be one of the high-priority items before us.

Human Resources Needs The human resources needed for a large project like INO are varied. Broadly they are classified as:

- Construction and installation: Mainly civil and mechanical engineers and scientists will be involved in the installation of the detector and data systems. While the civil and mechanical works will be entrusted to appropriate external agencies, INO will need its own engineers to ensure all design requirements are met.

- Maintainance and operations: After the installation of the detector, approximately about 15 engineers/scientists will be needed to ensure continuous running of the detector throughout the day.

- End-user groups: This groups consists of physicists—faculty/students/postdocs—who are members of the INO collaboration. A collaboration of this type needs at least 50 people including about 30 scientists. At any time about 15 members of this group will be present on-site conducting experiments and data analysis. Apart from these, there must be opportunities for students and visiting scientists to pursue short-term projects at the site.

The required human resources, scientific, may be generated in about four to five years time. Some strategies are outlined below.

INO Training School: One solution is to start a training school, either separately or attached to one of the existing training programs at BARC and CAT, that can train about 15 MSc/B.Tech/BE students every year at an all-India level, so that in 5 years we would have about 75 experimental physicists and some engineers with basic training. The trainees will be given jobs at one of the participating Institutions on the basis of successful performance in the training school.

The trainees would be taught relevant subjects such as high energy and nuclear physics, detector physics, computer simulation, data handling and analysis. There is enough expertise in the country to undertake such an endeavour. If desired, the scope of the training school may also be expanded to include all experimental HEP projects including the current neutrino project.

A Joint Universities Training Programme: Another possibility is to use the University system for this training programme. Many universities like Delhi University, Panjab University, Jammu University and University of Rajasthan already have an active experimental HEP programme. A joint universities training programme run by these HEP departments is yet another possibility.

Direct Recruitment: Actually, the best training could be imparted through hands-on experience in existing experiments on detector development activities, rather than class room teaching. On the basis of an all-India advertisement, about a dozen people could be recruited immediately. This can be repeated every year. Both physicists and engineers must be recruited.

Any one of these processes or a suitable combination of them must be initiated immediately.

Chapter 7

Cost and Time Schedules

We provide some ball-park estimates of the cost and time scales for various tasks. No detailed estimates are available at present and the figures mentioned in this chapter are very preliminary estimates.

7.1 Cost Factors

The cost factors include the following items; details are listed in Table 7.1.

- Site: Each of the sites involves construction of tunnels, laboratory cavern and support structures. The actual cost depends on the nature of rock, availability of labour and ease of access[1].

  The approximate cost for the construction at PUSHEP is Rs. 30 crores, which includes an access tunnel (dia. 7 m D-shaped) of length 2.2 kms and a cavern of dimensions 120 m $\times$ 20 m $\times$ 25 m (height). The length of the cavern has been chosen so as to accomodate up to 100 ktons of ICAL detector (that is, 6 modules of dimensions as described in Chapter 2).

  The corresponding figure for construction at Rammam is Rs. 80 crores, which includes a main access tunnel (dia. 7 m D-shaped) of length 4.85 kms, an adit (dia. 7 m D-shaped) of 2 kms and a cavern of the same dimensions as at PUSHEP.

  If the laboratory is located in Rohtang pass, there will a substantial saving since no access tunnel is required at this site.

- Civil Work: Some civil work will be needed at the point of access to tunnel portal, for structures to house the surface lab., and some buildings to house people who will work in the lab. The total cost of such civil work will be in the region of Rs. 35 crores; a break-up of the estimate is shown in Table 7.1. Furthermore, some facilities such as overhead-crane for lifting equipment and steel plates into place, air-circulation and air-conditioning in the lab and tunnel are required. This will cost roughly Rs. 20 crores.

- Detector: The detector will be built in modular form, each module having dimensions 16 m $\times$ 16 m $\times$ 12 m (height). The costs estimated below are for two modules (35 ktons), as envisaged in the first phase.

[1]The estimates given here are based on the budgetary estimates given by **L & T** Limited.

No.	Item	Cost (in crores of Rs.) PUSHEP	Rammam
I	LAB CONSTRUCTION (surface and underground)		
1.	Tunnel and cavern excavation	30	80
2.	Civil work underground and on surface	35	
	(i) for the tunnel road		
	(ii) in the cavern		
	(iii) at surface lab		
	(iv) for hostel buildings		
	(v) for flats/other accomodation		
3.	Facilities in the cavern	20	
	(i) overhead crane		
	(ii) air circulation in tunnel		
	(iii) air-conditioning the lab		
	(iv) electrical work		
	Total cost of lab construction	85	135
II	COST OF ICAL DETECTOR (two modules)		
	COST OF IRON		
4.	Iron (at Rs. 40 per kg)	140	
	Total cost of iron	140	140
III	OTHER DETECTOR-RELATED COST		
5.	Magnetisation	15	
6.	Detector	80	
	(i) RPC		
	(ii) strip plates		
	(iii) front-end electronics		
	(iv) power supply		
	(v) gas circulation system		
7.	Electronics and DAQ	20	
8.	Contingencies	30	
	Total detector-related cost (excl. iron)	145	145
	TOTAL	370	420

Table 7.1: Estimated total cost of INO underground laboratory and two modules (35 ktons) of ICAL detector at INO at the two possible sites, PUSHEP and Rammam. Where only one column is filled, the cost is the same at both sites. Note that the cost of iron is substantial but it can be re-used.

- Iron: A total of 35 ktons (or more) of iron rolled into plates is required for two moudules of ICAL. Normal mild steel costs around Rs. 40 per kg[2] and has a saturation magnetic field of about 1–1.4 Tesla. The cost of iron is expected to be around Rs. 140 crores. Here we have not taken into account the fact that if any special modification in the composition of steel is required for magnetisation purposes this will increase the cost further.

[2] The rate in 2003 was Rs. 20 per kg. A recent escalation of the costs has already driven this price up to about Rs. 40 per kg.

It may be noted that there is no degradation of iron—once the experiment is finished, it can be reused. **Even though this is one of the biggest components of the total expenditure of INO, it is a recoverable expenditure.**

- Magnetisation: Approximately Rs. 15 crores, including the cost of coils and machining.
- Detector: Approximately Rs. 80 crores for the detector elements including glass plates, strip plates, front-end electronics, power supply, gas system. The cost of a veto blanket of scintillators is not included here. NABA PLEASE CONFIRM THIS.
- Electronics and Data acquisition: Approximately Rs. 20 crores for DAQ, trigger, external veto, etc.

In summary, the total estimated cost of building the laboratory is around Rs. 85 (135) crores at PUSHEP (Rammam). This includes the cost of constructing a cavern that is big enough to contain a 100 kton iron calorimeter detector, that is, the size provides for future possible expansion. The cost of two modules of the ICAL detector is expected to be around Rs. 285 crores, of which Rs. 140 crores (for the iron) is recoverable and Rs. 30 crores has been added for contingencies. (The estimates for the site at Rohtang will be similar to PUSHEP or even less depending on the local geological information.) Hence, substantial cost goes into setting up the facilities at the surface as well as making the underground laboratory. Note that the underground laboratory will be a national facility and can be used for other types of experiments also. The break-up of costs is shown more conveniently in table form in Table 7.1.

The estimates given above do not include the operating cost at either of these sites. A major recurring expenditure is the cost of the gas mixture. However, in general, operating costs are site dependent.

7.2 Time Scale

The project may be executed in three phases once the approval is given in principle:

- Phase 1 of approximately 12–18 months duration: Site investigation to draw up detailed design reports for tunnel and cavern complex. This could be faster if all the permissions are easily available and and the work entrusted to reputed engineering group/s.

  Detailed design reports on the detector structure, RPC, pick-up electrodes, front-end electronics, power supply systems will be made available.

- Phase 2: Tunnel and cavern excavation, support measures, etc., to be put in place. The estimated time at PUSHEP is 22 months. The estimated time at Rammam is 41 months[3].

  The basic design of RPCs as already available will be frozen by this time. Tenders for the supply of iron, magnet coil, cables will be given. Manufacturing procedure for detector elements, electronics and gas mixing units will be frozen and the production process will be begun.

[3]Based on L & T estimates.

- Phase 3 of approximately 12–18 months duration. This period involves laboratory outfitting, transport of detector components and material and assembly. The first module may be completed early, and data taking begun. This phase ends with laboratory occupancy and data taking by the second module.

Chapter 8

INO as a facility for the future

In Chapter 3, a discussion of the main physics problems that are envisaged to be undertaken at INO with ICAL was given. ICAL is expected to be only the first detector to be put in the INO laboratory. In the future, INO is expected to house other neutrino detectors, especially for low energy neutrino detection. Apart from neutrino physics and neutrino astronomy, an underground laboratory offers possibilities for studies on several important and current problems in physics and other fields. After the closure of the laboratory at KGF there has been no such underground laboratory in the country. We recall the main advantages of such a laboratory:

- Low cosmic ray background as exemplified by Fig. 5.7. If the site has in addition low rock radioactivity, experiments requiring low background in high and low energy radiation can be undertaken.

- Reduction in the vibration levels due to surface activities.

We list some of the fields that can be profitably started and studied in such an underground laboratory:

- One of the interesting features that needs further study in connection with solar neutrinos is the day–night effect. A solar neutrino detector as close to the equator as possible is advantageous for such studies [36]. A heavy water detector is under consideration and the physics possibilities with such a detector are being analysed.

- Experiments involving neutrinos from nuclear reactors in the vicinity of such a laboratory can yield information on neutrino properties.

- A long term watch for neutrinos from stellar collapse (supernovae) can be undertaken from such a laboratory.

- About 40% of the heat outflow from the earth is estimated to be generated from terrestrial radioactivity, mainly from the decay of U^{238} and Th^{232}. There are several models for the distribution of these materials in the earth. These can be tested by studying low energy neutrinos in an underground laboratory [37].

- Neutrino tomography of the earth may be undertaken by studying matter effects on the phenomena of oscillation of neutrinos from laboratory sources and atmospheric neutrinos [38].

- Low background conditions like the ones obtainable in an underground laboratory with low rock radioactivity are required for studying important and rare processes like neutrinoless double decay. As already mentioned in the Introduction, such experiments (a few of which are already under operation) give important information on the Dirac or Majorana nature of neutrino. A Majorana mass as low as 0.2 eV or lower may be determined from such an experiment.

- There is continuing interest in low energy (up to a few hundred KeV) nuclear cross sections that are relevant in nuclear astrophysics such as the capture of α-particles on ^{12}C in stellar nucleosynthesis. A low energy high current accelerator in an underground laboratory (like LUNA in Gran-Sasso) with suitable low energy particle detectors can serve this purpose. Dark matter and dark energy searches are yet other possibilities in any underground laboratory.

- The low background conditions may be utilised to study detector and material development.

- The reduction of vibration due to surface activity can be helpful in the study of gravitational waves.

- Seismic studies, subsurface studies in life-sciences, nuclear test monitoring, etc., are possible.

It is obvious that there is a need for a well-equipped underground laboratory from several points of view. The realisation of the INO project can initiate such programmes in the country.

Bibliography

[1] The list of references on Standard Model and Neutrino oscillations is huge[1]. Here we give references to books and reviews where all the essential details needed for this report are available:
J.N. Bahcall, *Neutrino Astrophysics* (Cambridge Univ.Press, 1989);
G. Rajasekaran. *Phenomenology of neutrino oscillations*, *Pramana*, **55**, 19 (2000);
R. N. Mohapatra and Palash Pal, *Massive neutrinos in Physics and Astrophysics* (World Scientific, Singapore, 2004);
N.G. Cooper, Ed., *Celebrating the Neutrino*, Published in "Los Alamos Science", No. 25 (1997).
D. Indumathi, M.V.N. Murthy and G. Rajasekaran, Eds., *Perspectives in Neutrino Physics*, Proceedings of Indian National Science Academy **76** (2004).

[2] B. T. Cleveland *et al., Astrophys. J.* **496**, 505 (1998); Nucl. Phys. B (Proc. Suppl.) **38**, 47 (1995); W. Hampel *et al.*, (Gallex collaboration), *Phys. Lett.* **B447**, 127 (1999); J.N. Abdurashitov *et al.*, (SAGE collaboration), *Phys. Rev.* **C60**, 055801 (1999); M. Altmann *et al.*, (GNO collaboration), *Phys. Lett.* **B492**, 16 (2000); Y. Fukuda *et al.*, (Super-Kamiokande collaboration), *Phys Rev. Lett.* **82**, 2430 (1999); **86** 5651 (2001); Q. R. Ahmad *et al.*, (SNO collaboration), *ibid.* **87**, 071301 (2001); B. Aharmim *et al.*, (SNO Collaboration) hep-ex/0407029; M. B. Smy *et al.*, (Super-Kamiokande Collaboration), *Phys. Rev.* **D 69** (2004) 011104 [hep-ex/0309011]; S. N. Ahmed *et al.*, (SNO Collaboration), nucl-ex/0309004; J. Yoo *et al.*, (Super-Kamiokande Collaboration), *Phys. Rev.* **D 68** (2003) 092002 [hep-ex/0307070].

[3] Y. Fukuda *et al.*, (Super-Kamiokande Collaboration), *Phys. Rev. Lett.* **81** 1562 (1998) [hep-ex/9807003]; Y. Fukuda *et al.*, (Super-Kamiokande Collaboration),*Phys. Rev. Lett.* **82** 2644 (1999) [hep-ex/9812014]; W.W.M. Allison *et al.*, (Soudan-2 Collaboration), *Phys. Lett.* **B449** 137 (1999) [hep-ex/9901024]; M. Ambrosio *et al.*, (MACRO Collaboration), *Phys. Lett.* **B478** 5 (2000); S. Fukuda **et al.**, (Super-Kamiokande Collaboration), *Phys. Rev. Lett.* **85** 3999 (2000) [hep-ex/0009001]; M. Ambrosio *et al.*, (MACRO Collaboration), *Phys. Lett.* **B566** 35 (2003) [hep-ex/0304037]; M. Sanchez *et al.*, (Soudan 2 Collaboration), *Phys. Rev.* **D68** 113004 (2003) [hep-ex/0307069].

[4] Figure taken from the talk presented by P. Bhattacharjee at the Neutrino-2001 meeting, The Institute of Mathematical Sciences, Chennai, February 2001.

[5] Neutrino mass limits have been reviewed recently by
Carlo Giunti, hep-ph/0308206, NuFact 03, 5th International Workshop on Neutrino

[1]In order to keep this report concise, we have not given a complete list of references, but only a representative list to help the reader interested in further reading.

Factories & Superbeams, 2003; Christian Weinheimer, hep-ex/0306057, 10th Int. Workshop on Neutrino Telescopes, Venice/Italy, March 2003; Jean-Luc Vuilleumier, hep-ex/0306010, XXXVIII Rencontres de Moriond, Electroweak interactions and Unified Theories, 2003.

[6] S. Goswami, talk at Neutrino 2004, see S. Goswami, A. Bandyopadhyay and S. Choubey, arXiv:hep-ph/0409224.

[7] M.C. Gonzalez-Garcia, hep-ph/0410030, Nobel Symposium on Neutrino Physics.

[8] K.S. Hirata, *et al.*, (Kamiokande-II Collaboration), *Phys. Rev.* **D38** 448 (1988).

[9] R. Cisneros, *Astro. Sp. Sci.* **10**, 87 (1971); M. Voloshin, M. Vysotskii, L.B. Okun, *JETP* **64**, 446 (1986), *Sov. J. Nucl. Phys.* **44**, 440 (1986); for a recent review see, Yifang Wang, hep-ex/0411028, talk given at 32nd Intl. Conf. on High Energy Physics, 2004, Beijing, P.R. China.

[10] C. Athanassopoulos, *et al.* (LSND Collaboration), *Phys. Rev. Lett.* **81**, 1774 (1998); *Phys. Rev.* **C58**, 2489 (1998).

[11] Y. Ashie *et al.* (Super-Kamiokande Collaboration), hep-ex/0404034.

[12] G. Bhattacharyya, H.Pas, L. Song and T.J. Weilere, *Phys. Lett.* **B564**, 175 (2003) [hep-ph/0302191].

[13] The details of the MONOLITH proposal may be seen at http://castore.mib.infn.it/ monolith/.

[14] For a comprehensive list of ongoing, future experiments as well as theory of neutrino oscillations, solar neutrinos and atmospheric neutrinos, see The Neutrino Oscillation Industry page at http://www.hep.anl.gov/ndk/hypertext/nuindustry.html and follow the links; another useful site for comprehensive information on the status of neutrino physics is The Ultimate Neutrino page at http://cupp.oulu.fi/neutrino/.

[15] Detection of muons produced by cosmic ray neutrinos underground, C.V. Achar *et al.*, *Phys. Lett.* **18**, 196 (1965).

[16] M.R. Krishnaswamy, M.G.K. Menon, N.K. Mondal, V.S. Narasimham, B.V. Sreekantan, Y. Hayashi, N. Ito, S. Kawakami, S. Miyake (KGF Collab.) *Nuovo Cimento* **C9**, 167 (1986).

[17] M.R. Krishnaswamy *et al., Phys. Lett.* **B57**, 105 (1975); *Pramana*, **5**, 59 (1975).

[18] For details of the National Underground Science and Engineering Laboratory proposal see http://int.phys.washington.edu/NUSEL/.

[19] Some details of the INO proposal may be seen at http://www.imsc.res.in/∼ino.

[20] M.Anelli *et al., Nucl. Inst. and Meth.*, **A300** 572 (1991).

[21] Z. Maki, M. Nakazawa, S. Sakata, *Prog. Theor. Phys.* **28**, 870 (1962).

[22] M. Maltoni *et al.*, hep-ph/0405172.

[23] M. Apollonio *et al.* (CHOOZ Collaboration), *Phys. Lett.* **B466**, 415 (1999) [hep-ex/9907037].

[24] V. Agrawal, T. K. Gaisser, P. Lipari and T. Stanev, *Phys. Rev.* **D53**, 1314 (1996) [hep-ph/9509423].

[25] M. Honda, T. Kajita, K. Kasahara and S. Midorikawa, *Phys. Rev.* **D70**, 043008 (2004) [astro-ph/0404457].

[26] D. Indumathi and M.V.N. Murthy, hep-ph/0407336.

[27] A. Datta, R. Gandhi, P. Mehta and S. Uma Sankar, *Phys.Lett.* **B597**, 356 (2004) [hep-ph/0312027].

[28] V. D. Barger *et al.*, *Phys. Rev. Lett.* **85**, 5055 (2000) [hep-ph/0005197].

[29] T.D. Lee and C.N. Yang, *Phys. Rev.* **98** , 1501 (1955); L.B. Okun, *Sov. J. Nucl. Phys.* **10**, 206 (1969); for a review see A.D. Dolgov, *Phys. Rep.* **320**, 1 (1999).

[30] A.S. Joshipura and S. Mohanty, *Constraining long-range leptonic forces using iron calorimeter detectors*, PRL Preprint, October 2004.

[31] C. Albright *et al.*, hep-ex/0008064; see also the web site http://gate.hep.anl.gov/ndk/hypertext/nufactory.html for a complete listing of proposals around the world.

[32] R. Gandhi, P. Ghoshal, S. Goswami, P. Mehta and S. Uma Sankar, hep-ph/0408361 and work in progress.

[33] R. Saakian, *Nucl. Phys. Proc. Suppl.* **111**, 169 (2002).

[34] I. S. Alekseev and G. T. Zatsepin, Proc. Intl. Conf. on Cosmic Rays, Moscow, Vol.1, p.324, 1960; R. P. Kokoulin and A. A. Petrukhin, *NIM* **A263**, 468 (1988); R. P. Kokoulin and A. A. Petrukhin, *Sov. J. Part. Nucl.* **21**, 332 (1990).

[35] A. de Rujula *et al., Phys. Rev. Lett.* **35**, 628 (1975); G. Rajasekaran and K.V.L. Sarma, *Pramana* **5**, 78 (1975); J.C. Pati and A. Salam, Preprint ICTP/75/73, (1975).

[36] Mohan Narayan, G. Rajasekaran and Rahul Sinha, *Mod. Phys. Lett.* **A13**, 1915 (1998).

[37] See, for example, R.S. Raghavan *et al., Phys. Rev. Lett.* **80**, 635 (1998); H. Nunokawa *et al.,* hep-ph/0308175; F. Mantovani *et al.,* hep-ph/0309013; K. Eguchi *et al.,* (KamLAND Collab.) *Phys. Rev. Lett.* **90**, 021802 (2003); S. Mohanty, hep-ph/0302060; R.S. Raghavan, hep-ex/0208038.

[38] Neutrino tomography of the earth was proposed in A. De Rujula, S. Glashow, R. Wilson and G. Charpak, *Phys. Rep.* **99**, 341 (1983).

[39] P. Picchi and F. Pietropaolo, ICGF RAP. INT. 344/1997, Torino 1997 (CERN preprint SCAN-9710037).

[40] The NUANCE Neutrino Generator, D. Casper, *Nucl. Phys. Proc. Suppl.* **112** 161 (2002) (http://www.ps.uci.edu/∼nuint/nuance/default.htm).